

# Quantum decoherence in the Caldeira–Leggett model by the real-time path integral on a computer

---

Jun Nishimura,<sup>a,b</sup> Hiromasa Watanabe<sup>a,c</sup>

<sup>a</sup>*KEK Theory Center, Institute of Particle and Nuclear Studies,  
High Energy Accelerator Research Organization, 1-1 Oho, Tsukuba, Ibaraki 305-0801, Japan*

<sup>b</sup>*Graduate Institute for Advanced Studies, SOKENDAI, 1-1 Oho, Tsukuba, Ibaraki 305-0801, Japan*

<sup>c</sup>*Yukawa Institute for Theoretical Physics, Kyoto University, Kyoto 606-8502, Japan*

*E-mail:* [jnishi@post.kek.jp](mailto:jnishi@post.kek.jp), [hiromasa.watanabe@yukawa.kyoto-u.ac.jp](mailto:hiromasa.watanabe@yukawa.kyoto-u.ac.jp)

**ABSTRACT:** We propose first-principle calculations of an open system based on the real-time path integral formalism treating the environment as well as the system of our interest together on a computer. The sign problem that occurs in applying Monte Carlo methods can be overcome in general by using the so-called Lefschetz thimble method, which has been developed over the past decade. Here we focus on the Caldeira–Leggett model, which is well known, in particular, as a model of quantum decoherence. In this case, the calculation simplifies drastically since the path integral becomes Gaussian for typical initial conditions. The relevant saddle point, which is unique and complex, can be determined by solving a linear equation with a huge but sparse coefficient matrix, and the integration over the Lefschetz thimble can be performed analytically. Thus we obtain, without assumptions or approximations, the reduced density matrix after a long-time evolution, tracing out a large number of harmonic oscillators in the environment. In particular, we confirm the dependence of the decoherence time on the coupling constant and the temperature that has been predicted from the master equation in a certain parameter regime.

---

## Contents

<b>1</b>	<b>Introduction</b>	<b>1</b>
<b>2</b>	<b>Brief review of decoherence in the Caldeira–Leggett model</b>	<b>4</b>
<b>3</b>	<b>The real-time path integral with discretized time</b>	<b>9</b>
3.1	Choosing the parameters of the model	9
3.2	The effective action for the Caldeira–Leggett model	11
3.3	Performing the path integral by the Gaussian integral	12
<b>4</b>	<b>Numerical results for a single wave packet</b>	<b>14</b>
4.1	Increasing the number of harmonic oscillators	15
4.2	Dependence on the coupling and the temperature	17
4.3	Dependence on the cutoff frequency $\omega_{\text{cut}}$	20
<b>5</b>	<b>Numerical results for the “double-slit experiment”</b>	<b>21</b>
5.1	Extending the calculations to two wave packets	21
5.2	The effect of decoherence on the interference pattern	24
<b>6</b>	<b>Summary and discussions</b>	<b>28</b>
<b>A</b>	<b>Discretization effects due to finite lattice spacing <math>\epsilon</math> and finite <math>N_{\mathcal{E}}</math></b>	<b>29</b>
<b>B</b>	<b>More on decoherence for two wave packets</b>	<b>30</b>

---

## 1 Introduction

Quantum mechanics is one of the most successful theories in physics, which enables us to understand various nontrivial phenomena that occur in our Universe. In particular, since the dawn of quantum mechanics in 1920s, experiments on microscopic or even mesoscopic systems have become gradually possible, and the theory of measurements in quantum mechanics has developed significantly. Nowadays it is widely recognized that the presence of the measuring device and the environment cannot be ignored since they disturb the system through interactions and the subsequent entanglement. Tracing out the environment after the measurement disables the interference that the system can potentially exhibit. This effect, which is called *quantum decoherence* (See *e.g.*, Refs. [1, 2]), plays a crucial role in accounting for the outcome of measurements consistently by calculations in quantum mechanics. Since decoherence is a source of quantum noise in quantum computation

and experiments such as the gravitational wave detection which use quantum technologies, realistic modeling of the influence by the environment is important in reducing the uncontrollable uncertainties due to the noise.

Theoretically, the decoherence can be expressed as the disappearance of the off-diagonal elements of the density matrix in a basis associated with the measurement during the time evolution, which causes the quantum-to-classical transition. Thus the decoherence is important in interpreting the “collapse of wave functions” properly as well as in answering fundamental questions such as “How does the microscopic quantum theory turn into the macroscopic classical theory, which describes our real world?” [1, 2].

A common strategy for studying a system coupled to some environment is to use the master equation [3, 4] that describes the non-unitary time evolution of the reduced density matrix of the system after tracing out the environment. (See also Section 4 of Ref. [1] and references therein.) However, master equations are obtained in general only under some assumptions such as high temperature with some approximations such as the Born and Markov approximations. It is therefore desirable to develop alternative methods that do not rely on such assumptions and approximations.

As a possible approach, one can think of investigating the unitary time evolution of the whole system including the environment either by solving the Schrödinger equation or by evaluating the Feynman path integral. The first option has been pursued in the context of decoherence, for instance, in Refs. [5, 6]. However, the required computational cost is similar to that for diagonalizing the Hamiltonian, and it grows exponentially with the number of degrees of freedom in the whole system. Here we consider the second option, namely evaluating the path integral based on Monte Carlo (MC) simulation,<sup>1</sup> which has a potential to reduce the computational cost to a power-law growth. The obstacle in that case is the notorious sign problem due to the oscillating phase in the integrand. See Refs. [10–20] for recent development in the path integral approach to the real-time quantum evolution.

MC simulation is a well-established practical method to evaluate a multi-variable integral. The idea is to generate variables, let’s say  $\Phi$ , with the probability density proportional to the Boltzmann weight  $e^{-S[\Phi]}$  with the action  $S[\Phi]$  and to compute the expectation values. This method is based on the fact that the action  $S[\Phi]$  is real so that the Boltzmann weight can be regarded as the probability density. When the action becomes complex, a naive implementation of the MC method becomes problematic. A straightforward approach would be to use the reweighting method in which one generates the ensemble with the probability density  $e^{-\text{Re} S[\Phi]}$  and includes the effects of the complex phase  $e^{-i \text{Im} S[\Phi]}$  in evaluating the expectation values. Unfortunately, this complex phase becomes highly oscillatory as the system size increases, and forces us to generate a prohibitively large number of sample configurations by MC to estimate physical quantities with sufficient precision. This is called the sign problem.

The situation with the sign problem has drastically changed over the last decades, however. It has been widely recognized that a promising way to overcome the problem

---

<sup>1</sup>Apart from evaluating the real-time path integral numerically by Monte Carlo methods, there is also an analytic approach based on perturbation theory, which enables us to calculate the time evolution of the reduced density matrix in quantum field theories [7–9].

is to complexify the integration variables and to deform the integration contour based on Cauchy's theorem in such a way that the sign problem is ameliorated. The Lefschetz thimble method [21–24] is a typical method in that direction. In particular, after the proposal of the generalized Lefschetz thimble method (GTM) [25], various important techniques have been developed [26–32], which enabled, for instance, the investigation of quantum tunneling [11], quantum cosmology [33] and string theory [34] based on the real-time path integral. It is expected that this method is useful also in investigating a system coupled to its environment since the computational cost grows only by a power law with the system size  $V$ . More precisely, the generation of sample configurations requires the cost of  $O(V)$ , whereas the calculation of the Jacobian for reweighting requires the cost of  $O(V^3)$ .

As a first step towards such calculations, we focus on the Caldeira–Leggett (CL) model [35, 36], which has been studied intensively in investigating decoherence and dissipation in quantum systems [37–39] although it was originally proposed to describe the quantum Brownian motion. See also a textbook [1], reviews [40, 41], and references therein. In fact, the calculations simplify in this case drastically since the path integral to be evaluated for typical initial conditions is nothing but a multi-variable Gaussian integral. The relevant saddle point, which is unique and complex, can be determined by solving a linear equation with a huge but sparse coefficient matrix, and the integration over the Lefschetz thimble can be performed analytically. Thus we obtain, without assumptions or approximations, the reduced density matrix after a long-time evolution, tracing out a large number of harmonic oscillators in the environment.

The purpose of this paper is to confirm the usefulness of our formalism by reproducing the nature of decoherence in the CL model predicted from the master equation. For that, we discuss in detail the correspondence between the parameters in the master equation and those in our formalism, and confirm the scaling with respect to the number of harmonic oscillators in the environment. In particular, we focus on the high temperature and weak coupling region, where the description by the master equation is expected to be valid qualitatively. Our results indeed confirm the dependence of the decoherence time on the parameters of the model which is predicted by the master equation. Let us stress, however, that our method is applicable to a general parameter region in which the master equation is not valid. We also observe the thermalization of the system of our interest into a canonical distribution due to the interaction with the environment. Thus this work paves the way to a new possibility of investigating the time evolution of an open quantum system by performing the real-time path integral of the whole system including the environment numerically. Part of our results were reported briefly in our previous publication [42] emphasizing our finding that quantum decoherence can be captured by complex saddle points just like quantum tunneling can be captured by instantons, which are real saddle points in the imaginary-time path integral formalism. (See also Ref. [11] for a new picture of quantum tunneling based on complex saddle points in the real-time path integral formalism.)

The rest of this paper is organized as follows. In Section 2, we first review the CL model and discuss its properties concerning quantum decoherence based on the master equation. In Section 3, we discuss how to perform the real-time path integral for the

model with discretized time and a finite number of harmonic oscillators. In Section 4, we show our numerical results for a single wave packet, and discuss how the decoherence takes place in that case. In Section 5, we discuss how to extend our calculations to the case of two wave packets analogous to the double-slit experiment and show our numerical results, which clearly indicate the effects of decoherence as the fading of the interference pattern. Section 6 is devoted to a summary and discussions. In Appendix A, we discuss the effect of finite lattice spacing introduced in discretizing time and that of using a finite number of harmonic oscillators in the environment, which discretizes their frequency spectrum. In Appendix B, we discuss the decoherence for the two wave packets from the viewpoint of the off-diagonal elements of the reduced density matrix.

## 2 Brief review of decoherence in the Caldeira–Leggett model

The Caldeira–Leggett (CL) model [35, 36] was originally introduced to describe the quantum Brownian motion, which is caused by the effect of friction in a quantum system. After the original work, it was pointed out that this model also exhibits significant quantum decoherence [37]. In this section, we briefly review the CL model and its properties concerning quantum decoherence based on Ref. [35]. Although our discussion shall be given in the path integral formalism, which is used in our numerical method later on, similar discussions are also possible in the operator formalism as one can see in Ref. [43], for instance. For more comprehensive reviews, see Refs. [1, 41, 44–46].

The CL model is defined by the Hamiltonian

$$H = H_0 + H_{\mathcal{E}} + H_{\text{int}} , \quad (2.1)$$

$$H_0 = \frac{p^2}{2M} + V(x) , \quad H_{\mathcal{E}} = \sum_{k=1}^{N_{\mathcal{E}}} \left( \frac{p_k^2}{2m} + \frac{1}{2} m \omega_k^2 q_k^2 \right) , \quad H_{\text{int}} = -x \sum_{k=1}^{N_{\mathcal{E}}} c_k q_k , \quad (2.2)$$

where  $N_{\mathcal{E}}$  represents the number of harmonic oscillators in the environment  $\mathcal{E}$ , and  $c_k$  are the coupling constants between the system  $\mathcal{S}$  and the environment  $\mathcal{E}$ . In what follows, we assume that the system  $\mathcal{S}$  is also a harmonic oscillator defined by

$$V(x) = \frac{1}{2} M \omega_b^2 x^2 , \quad (2.3)$$

where  $\omega_b$  represents the “bare” frequency as opposed to the “renormalized” one defined later in (2.29). We also assume that the initial condition for the density matrix is given by

$$\hat{\rho}(t=0) = \hat{\rho}_{\mathcal{S}}(0) \otimes \hat{\rho}_{\mathcal{E}}(0) , \quad (2.4)$$

meaning that  $\mathcal{S}$  and  $\mathcal{E}$  are separable. The initial density matrix  $\hat{\rho}_{\mathcal{S}}(0)$  for the system  $\mathcal{S}$  shall be specified later (3.15), whereas the initial density matrix  $\hat{\rho}_{\mathcal{E}}(0)$  for the environment is assumed to be the canonical ensemble with the temperature  $T = \beta^{-1}$ .

In view of the form of the interaction term  $H_{\text{int}}$  in (2.2), we will work in the position basis in what follows. In particular, the initial density matrix  $\hat{\rho}_{\mathcal{E}}(0)$  for the environment

can be written explicitly as<sup>2</sup>

$$\rho_{\mathcal{E}}(q, \tilde{q}; 0) = \langle \tilde{q} | \hat{\rho}_{\mathcal{E}}(0) | q \rangle = \prod_{k=1}^{N_{\mathcal{E}}} \rho_{\mathcal{E}}^{(k)}(q_k, \tilde{q}_k) , \quad (2.5)$$

$$\rho_{\mathcal{E}}^{(k)}(q_k, \tilde{q}_k) = \sqrt{\frac{m\omega_k}{2\pi \sinh \beta\omega_k}} \exp \left[ -\frac{m\omega_k}{2 \sinh \beta\omega_k} \{ (q_k^2 + \tilde{q}_k^2) \cosh \beta\omega_k - 2q_k \tilde{q}_k \} \right] . \quad (2.6)$$

Note that Eq. (2.6) is nothing but the propagator for harmonic oscillators along the imaginary time and can be derived, e.g., from Mehler's formula. On the other hand, the total density matrix for the whole system obeys the time evolution given by

$$\rho(x, q; \tilde{x}, \tilde{q}; t) = \langle x, q | \hat{\rho}(t) | \tilde{x}, \tilde{q} \rangle = \langle x, q | e^{-i\hat{H}t} \hat{\rho}(0) e^{i\hat{H}t} | \tilde{x}, \tilde{q} \rangle . \quad (2.7)$$

Inserting the complete set of basis, we obtain

$$\rho(x, q; \tilde{x}, \tilde{q}; t) = \int dx' d\tilde{x}' dq' d\tilde{q}' \langle x, q | e^{-i\hat{H}t} | x', q' \rangle \langle x', q' | \hat{\rho}(0) | \tilde{x}', \tilde{q}' \rangle \langle \tilde{x}', \tilde{q}' | e^{i\hat{H}t} | \tilde{x}, \tilde{q} \rangle , \quad (2.8)$$

which can be rewritten further by using the propagator

$$\langle x, q | e^{-i\hat{H}t} | x', q' \rangle = \int \mathcal{D}x \mathcal{D}q e^{iS[x(t), q(t)]} , \quad (2.9)$$

where the action is given by

$$S[x, q] = S_0[x] + S_{\mathcal{E}}[q] + S_{\text{int}}[x, q] , \quad (2.10)$$

$$S_0[x] = \int_0^t d\tau \left\{ \frac{1}{2} M \dot{x}(\tau)^2 - \frac{1}{2} M \omega_b^2 x^2 \right\} , \quad (2.11)$$

$$S_{\mathcal{E}}[q] = \int_0^t d\tau \sum_{k=1}^{N_{\mathcal{E}}} \left\{ \frac{1}{2} m \dot{q}_k(\tau)^2 - \frac{1}{2} m \omega_k^2 q_k(\tau)^2 \right\} , \quad (2.12)$$

$$S_{\text{int}}[x, q] = \int_0^t d\tau x(\tau) \sum_{k=1}^{N_{\mathcal{E}}} c_k q_k(\tau) . \quad (2.13)$$

We have defined  $\dot{x}(\tau) \equiv dx(\tau)/d\tau$ ,  $\dot{q}_k(\tau) \equiv dq_k(\tau)/d\tau$  and the boundary conditions are given by  $x(0) = x'$ ,  $x(t) = x$ ,  $q(0) = q'$  and  $q(t) = q$ . The other factor  $\langle \tilde{x}', \tilde{q}' | e^{i\hat{H}t} | \tilde{x}, \tilde{q} \rangle$  in (2.8) can be rewritten in a similar way.

In order to investigate the decoherence, we trace out the environment by integrating out all the degrees of freedom in  $\mathcal{E}$ , and obtain the reduced density matrix of  $\mathcal{S}$  as

$$\rho_{\mathcal{S}}(x_{\text{F}}, \tilde{x}_{\text{F}}; t) = \int dq \langle x_{\text{F}}, q | \hat{\rho}(t) | \tilde{x}_{\text{F}}, q \rangle = \int dx_{\text{I}} d\tilde{x}_{\text{I}} J(x_{\text{F}}, \tilde{x}_{\text{F}}; t; x_{\text{I}}, \tilde{x}_{\text{I}}; 0) \rho_{\mathcal{S}}(x_{\text{I}}, \tilde{x}_{\text{I}}; t=0) , \quad (2.14)$$

where the propagator for the reduced density matrix is given by

$$J(x_{\text{F}}, \tilde{x}_{\text{F}}; t; x_{\text{I}}, \tilde{x}_{\text{I}}; 0) = \int \mathcal{D}x \mathcal{D}\tilde{x} e^{i(S_0[x] - S_0[\tilde{x}])} e^{-W(x, \tilde{x})} \quad (2.15)$$

---

<sup>2</sup>Throughout this paper, we set  $\hbar = 1$ .

with the boundary conditions  $x(0) = x_I$ ,  $x(t) = x_F$  and  $\tilde{x}(0) = \tilde{x}_I$ ,  $\tilde{x}(t) = \tilde{x}_F$ . We have defined the Feynman–Vernon influence functional [47]

$$e^{-W(x, \tilde{x})} = \int \mathcal{D}q \mathcal{D}\tilde{q} \exp [i(S_{\mathcal{E}}[q] - S_{\mathcal{E}}[\tilde{q}] + S_{\text{int}}[x, q] - S_{\text{int}}[\tilde{x}, \tilde{q}])] \rho_{\mathcal{E}}(q(0), \tilde{q}(0); 0) , \quad (2.16)$$

which contains all the effect of the environment  $\mathcal{E}$  that has been traced out. Here the path integral is performed over the variables in the environment  $q$  and  $\tilde{q}$  with the boundary condition  $q(t) = \tilde{q}(t)$ .

In the case at hand with the initial condition (2.5), the path integral (2.16) can be evaluated explicitly as [35, 47]

$$W(x, \tilde{x}) = \int_0^t d\tau \int_0^\tau ds \{x(\tau) - \tilde{x}(\tau)\} \{\alpha(\tau - s)x(s) - \alpha^*(\tau - s)\tilde{x}(s)\} , \quad (2.17)$$

where the kernel  $\alpha(\tau)$  is given by

$$\text{Re } \alpha(\tau) = \sum_{k=1}^{N_{\mathcal{E}}} \frac{c_k^2}{2m\omega_k} \coth\left(\frac{\beta\omega_k}{2}\right) \cos(\omega_k\tau) , \quad \text{Im } \alpha(\tau) = - \sum_{k=1}^{N_{\mathcal{E}}} \frac{c_k^2}{2m\omega_k} \sin(\omega_k\tau) . \quad (2.18)$$

Plugging this in (2.15), we can rewrite the propagator  $J(x_F, \tilde{x}_F; t; x_I, \tilde{x}_I; 0)$  in the form

$$J(x_F, \tilde{x}_F; t; x_I, \tilde{x}_I; 0) = \int \mathcal{D}x \mathcal{D}\tilde{x} e^{i(S_0[x] - S_0[\tilde{x}])} e^{-iW_I(x, \tilde{x}; t) - W_R(x, \tilde{x}; t)} , \quad (2.19)$$

$$W_R(x, \tilde{x}; t) = \int_0^t d\tau \int_0^\tau ds \{x(\tau) - \tilde{x}(\tau)\} \text{Re } \alpha(\tau - s) \{x(s) - \tilde{x}(s)\} , \quad (2.20)$$

$$W_I(x, \tilde{x}; t) = \int_0^t d\tau \int_0^\tau ds \{x(\tau) - \tilde{x}(\tau)\} \text{Im } \alpha(\tau - s) \{x(s) + \tilde{x}(s)\} . \quad (2.21)$$

Note that the influence functional given by (2.20) and (2.21) involves integration over  $\tau$  and  $s$ , which implies that it is non-local with respect to time. We can simplify it by taking the  $N_{\mathcal{E}} \rightarrow \infty$  limit as follows. First we introduce the spectral density as

$$\rho(\omega) = \sum_{k=1}^{N_{\mathcal{E}}} \delta(\omega - \omega_k) , \quad \rho(\omega) C(\omega)^2 = \sum_{k=1}^{N_{\mathcal{E}}} c_k^2 \delta(\omega - \omega_k) , \quad (2.22)$$

and rewrite the sums in (2.18) as

$$\text{Re } \alpha(\tau) = \int_0^\infty d\omega \frac{\rho(\omega) C(\omega)^2}{2m\omega} \coth\left(\frac{\beta\omega}{2}\right) \cos(\omega\tau) , \quad (2.23)$$

$$\text{Im } \alpha(\tau) = - \int_0^\infty d\omega \frac{\rho(\omega) C(\omega)^2}{2m\omega} \sin(\omega\tau) . \quad (2.24)$$

Let us assume a specific form of the density called the Ohmic spectrum<sup>3</sup> as

$$\rho(\omega) C^2(\omega) = \begin{cases} 8mM\gamma\omega^2/(2\pi) & \omega \leq \omega_{\text{cut}} , \\ 0 & \omega > \omega_{\text{cut}} , \end{cases} \quad (2.25)$$

---

<sup>3</sup>The reason for being Ohmic can be seen from the fact that the spectral density  $J(\omega) = \sum_k \frac{c_k^2}{2m_k\omega_k} \delta(\omega - \omega_k)$ , which is used in standard textbooks instead of (2.22), becomes linear  $J(\omega) \propto \omega$  for  $\omega \leq \omega_{\text{cut}}$ .

which simplifies the kernel  $\alpha(\tau)$  and validates the Markov approximation [1, 41]. Within this assumption, there are still two parameters  $\gamma$ , and  $\omega_{\text{cut}}$ . Note that  $\gamma$  governs the strength of the coupling between the system and the environment. As we will see shortly in (2.29), the cutoff frequency  $\omega_{\text{cut}}$ , as well as  $\gamma$ , appears in the physical parameters of the system as the “renormalization” of the frequency.

Under the assumption (2.25), the imaginary part of the kernel (2.24) becomes

$$\text{Im } \alpha(\tau) = -4M\gamma \int_0^{\omega_{\text{cut}}} \frac{d\omega}{2\pi} \omega \sin(\omega\tau) = 2M\gamma \frac{d}{d\tau} f(\tau) , \quad (2.26)$$

where we have defined

$$f(\tau) = \int_{-\omega_{\text{cut}}}^{\omega_{\text{cut}}} \frac{d\omega}{2\pi} \cos(\omega\tau) , \quad (2.27)$$

which can be approximated by the delta function  $\delta(\tau)$  for  $\omega_{\text{cut}} \gg 1/\tau_0$  with  $\tau_0$  being the typical time resolution. Then the integral over  $s$  in (2.21) can be performed by parts as

$$\begin{aligned} W_I(x, \tilde{x}; t) &\approx -2M\gamma \int_0^t d\tau \left[ \{x^2(\tau) - \tilde{x}^2(\tau)\} f(0) - \frac{1}{2} \{x(\tau) - \tilde{x}(\tau)\} \{\dot{x}(\tau) + \dot{\tilde{x}}(\tau)\} \right] \\ &\approx -\frac{2M\gamma \omega_{\text{cut}}}{\pi} \int_0^t d\tau \{x^2(\tau) - \tilde{x}^2(\tau)\} + M\gamma \int_0^t d\tau \{x(\tau) - \tilde{x}(\tau)\} \{\dot{x}(\tau) + \dot{\tilde{x}}(\tau)\} , \end{aligned} \quad (2.28)$$

where we have used  $f(0) = \omega_{\text{cut}}/\pi$ . Note that the first term can be absorbed by shifting the parameter  $\omega_{\text{b}}^2$  of the potential (2.3) in  $S_0[x]$  and  $S_0[\tilde{x}]$  that appear in (2.19) as

$$\omega_{\text{r}}^2 = \omega_{\text{b}}^2 - (\Delta\omega)^2 , \quad (\Delta\omega)^2 = \frac{4\gamma \omega_{\text{cut}}}{\pi} . \quad (2.29)$$

Thus, this term corresponds to “renormalization” of the parameter in the original Hamiltonian due to the presence of the environment. This issue shall be discussed in the next section from a more general point of view.

Similarly the real part of the kernel (2.23) simplifies under the assumption (2.25) as

$$\text{Re } \alpha(\tau) = 4M\gamma \int_0^{\omega_{\text{cut}}} \frac{d\omega}{2\pi} \omega \coth\left(\frac{\beta\omega}{2}\right) \cos(\omega\tau) \approx \frac{4M\gamma}{\beta} f(\tau) , \quad (2.30)$$

where we have used  $\coth\left(\frac{\beta\omega}{2}\right) \approx \frac{2}{\beta\omega}$  assuming  $\beta\omega_{\text{cut}} \ll 1$  [35]. Then the integral over  $s$  in (2.20) can be performed as

$$\begin{aligned} W_R(x, \tilde{x}; t) &= \frac{4M\gamma}{\beta} \int d\tau ds \{x(\tau) - \tilde{x}(\tau)\} f(\tau - s) \{x(s) - \tilde{x}(s)\} \\ &\approx \frac{2M\gamma}{\beta} \int_0^t d\tau \{x(\tau) - \tilde{x}(\tau)\}^2 , \end{aligned} \quad (2.31)$$

where we have approximated (2.27) by the delta function again.



Using (2.28) and (2.31), the propagator (2.19) for the reduced density matrix becomes [35, 47],

$$\begin{aligned} J(x_F, \tilde{x}_F; t; x_I, \tilde{x}_I; 0) \\ = \int \mathcal{D}x \mathcal{D}\tilde{x} \exp \left[ iS_r[x] - iS_r[\tilde{x}] - iM\gamma \int_0^t d\tau \{x(\tau) - \tilde{x}(\tau)\} \{\dot{x}(\tau) + \dot{\tilde{x}}(\tau)\} \right] \\ \times \exp \left[ -\frac{2M\gamma}{\beta} \int_0^t d\tau \{x(\tau) - \tilde{x}(\tau)\}^2 \right], \end{aligned} \quad (2.32)$$

where the effect of the renormalization appears in the action as

$$S_r[x] = \frac{1}{2}M\dot{x}^2 - \frac{1}{2}M\omega_r^2 x^2, \quad (2.33)$$

which is obtained by replacing  $\omega_b^2$  in  $S_0[x]$  by (2.29).

Plugging the obtained propagator (2.32) in (2.14), one can deduce the master equation for the time evolution of the reduced density matrix as<sup>4</sup>

$$\frac{d}{dt}\rho_S(x, \tilde{x}; t) = K(x, \tilde{x})\rho_S(x, \tilde{x}, t), \quad (2.35)$$

$$K(x, \tilde{x}) = \frac{i}{2M} \left( \frac{\partial^2}{\partial x^2} - \frac{\partial^2}{\partial \tilde{x}^2} \right) - \frac{i}{2}M\omega_r^2(x^2 - \tilde{x}^2) - \gamma(x - \tilde{x}) \left( \frac{\partial}{\partial x} - \frac{\partial}{\partial \tilde{x}} \right) - \frac{2M\gamma}{\beta}(x - \tilde{x})^2. \quad (2.36)$$

The first two terms correspond to the standard Liouville-von Neumann terms describing the unitary evolution. The third term describes the dissipation due to the momentum damping, where its typical time scale is controlled by the effective coupling  $\gamma$ .

At high temperature (small  $\beta$ ), the last term dominates in the master equation (2.36), and one obtains

$$\frac{d}{dt}\rho_S(x, \tilde{x}; t) \sim -\frac{2M\gamma}{\beta}(x - \tilde{x})^2 \rho_S(x, \tilde{x}; t), \quad (2.37)$$

which implies the behavior

$$\rho_S(x, \tilde{x}; t) = \rho_S(x, \tilde{x}; 0) e^{-\frac{2M\gamma}{\beta}(x - \tilde{x})^2 t}. \quad (2.38)$$

Thus the off-diagonal elements of the density matrix in the position basis decay exponentially with time. This corresponds to the decoherence caused by the environment, where its typical time scale  $\tau_d$  can be defined by

$$\tau_d^{-1}(x, \tilde{x}) = \frac{2M\gamma}{\beta}(x - \tilde{x})^2 = \gamma \left( \frac{x - \tilde{x}}{\lambda_{dB}} \right)^2. \quad (2.39)$$

---

<sup>4</sup>This master equation can be expressed in a simpler form in the operator formalism [1, 41, 43] as

$$\frac{d\hat{\rho}_S(t)}{dt} = -i[\hat{H}_r, \hat{\rho}_S(t)] - i\gamma[\hat{x}, \{\hat{p}, \hat{\rho}_S(t)\}] - \frac{2M\gamma}{\beta}[\hat{x}, [\hat{x}, \hat{\rho}_S(t)]], \quad (2.34)$$

where the Hamiltonian  $\hat{H}_r$  is defined as  $\hat{H}_r = \hat{H}_0 - \frac{1}{2}M(\Delta\omega)^2 x^2$  with the shifted frequency (2.29). We should also mention that this master equation does not maintain the positivity of the reduced density matrix due to the high temperature approximation. The positivity can be recovered [48, 49], however, by adding an  $O(\beta)$  term  $\propto \gamma\beta[\hat{p}, [\hat{p}, \hat{\rho}_S(t)]]$ , which makes the master equation of the Lindblad type.

Here we have defined the thermal de Broglie wavelength  $\lambda_{\text{dB}} = \sqrt{\beta/2M}$  of the particle with mass  $M$  under temperature  $T = \beta^{-1}$ . Let us emphasize that the decoherence time  $\tau_d$  becomes shorter for longer distance between the positions  $x$  and  $\tilde{x}$ .

One of our main purposes of this work is to investigate the decoherence from first-principle calculations and to confirm, in particular, the formula (2.39) obtained above from the master equation. The importance of this is clear since the simple form of the master equation (2.36) for the reduced density matrix  $\rho_S(x, \tilde{x})$  is arrived at only with a specific setup and some assumptions. In particular, in order to validate the Markov approximation, we have taken the large  $N_{\mathcal{E}}$  limit assuming a specific form of the spectral density (2.25) for the environment and imposed a condition  $1/\tau_0 \ll \omega_{\text{cut}} \ll \beta^{-1}$ , where  $\tau_0$  is the typical time resolution. While the simple master equation derived in this way is indeed useful in understanding the non-unitary and dissipative dynamics of the system, it is important to clarify how and to what extent such behaviors are realized in the unitary time-evolution of the whole system, *i.e.*, the system  $\mathcal{S}$  and the environment  $\mathcal{E}$ .

### 3 The real-time path integral with discretized time

In this section, we first discuss how we discretize the Caldeira-Leggett model in the real-time path integral formalism in a way which is useful in comparing our results with the decoherence predicted by the master equation. Then we explain how to perform explicit calculations in the discretized model.

#### 3.1 Choosing the parameters of the model

The Lagrangian corresponding to the Hamiltonian (2.1) is given by

$$L = L_S + L_{\mathcal{E}} + L_{\text{int}} , \quad (3.1)$$

$$L_S = \frac{1}{2} \dot{x}^2 - \frac{1}{2} \omega_b^2 x^2 , \quad L_{\mathcal{E}} = \sum_{k=1}^{N_{\mathcal{E}}} \left\{ \frac{1}{2} (\dot{q}^k)^2 - \frac{1}{2} \omega_k^2 (q^k)^2 \right\} , \quad L_{\text{int}} = c x \sum_{k=1}^{N_{\mathcal{E}}} q^k , \quad (3.2)$$

where we denote the coordinate of the  $k$ -th harmonic oscillator as  $q^k$  with the upper suffix from now on reserving the lower suffix for the discretized time. We set the coupling constants  $c_k$  between the system  $\mathcal{S}$  and the  $k$ -th harmonic oscillator in the environment  $\mathcal{E}$  to a constant  $c$  since the results in the large  $N_{\mathcal{E}}$  limit with the spectral density (2.22) depends only on the combination  $\rho(\omega)C(\omega)^2$ , which implies that one can fix  $C(\omega) = c$  without loss of generality.<sup>5</sup> We have also absorbed the mass parameters  $M$  and  $m$  in (2.10) by rescaling  $x \rightarrow x/\sqrt{M}$ ,  $q^k \rightarrow q^k/\sqrt{m}$  and  $c \rightarrow c\sqrt{Mm}$ .

The frequencies  $\omega_k$  of the harmonic oscillators in the environment can be determined by requiring that the Ohmic spectrum (2.25) is reproduced in the large  $N_{\mathcal{E}}$  limit. For that, we introduce a function  $\omega = g(\kappa)$  of  $\kappa = \frac{k}{N_{\mathcal{E}}}$ , which gives  $d\omega = (dg/d\kappa) d\kappa$ . Since the distribution of the harmonic oscillators with respect to  $\kappa$  is uniform, the Ohmic spectrum

---

<sup>5</sup>This is true for any form of the spectral density, and it does not have to be the specific form (2.25).

(2.25) is reproduced if

$$\left(\frac{dg}{d\kappa}\right)^{-1} \propto \omega^2 = g(\kappa)^2, \quad (3.3)$$

which implies  $g(\kappa) \propto \kappa^{1/3}$ . Thus we obtain

$$\omega_k = \omega_{\text{cut}} \left(\frac{k}{N_{\mathcal{E}}}\right)^{1/3}, \quad (3.4)$$

where  $\omega_{\text{cut}}$  is the cutoff parameter introduced in (2.25). The spectral density one obtains in the large  $N_{\mathcal{E}}$  limit is given by

$$\rho(\omega) = \frac{3N_{\mathcal{E}}}{\omega_{\text{cut}}^3} \omega^2, \quad \rho(\omega) C(\omega)^2 = \frac{3c^2 N_{\mathcal{E}}}{\omega_{\text{cut}}^3} \omega^2, \quad (3.5)$$

where  $\omega \leq \omega_{\text{cut}}$ . Comparing (3.5) with (2.25), one obtains the asymptotic behavior of the coupling constant  $c$  at large  $N_{\mathcal{E}}$  as

$$c^2 \sim \frac{4\omega_{\text{cut}}^3}{3\pi N_{\mathcal{E}}} \gamma. \quad (3.6)$$

In order to determine the coupling constant  $c$  at finite  $N_{\mathcal{E}}$ , we reconsider the physical origin of the shift (2.29) in the frequency. For that, we complete the square with respect to  $q^k$  in the Lagrangian (3.2) as

$$L = \frac{1}{2} \dot{x}^2 - \frac{1}{2} \tilde{\omega}_{\text{r}}^2 x^2 + \sum_{k=1}^{N_{\mathcal{E}}} \left[ \frac{1}{2} (\dot{q}^k)^2 - \frac{1}{2} \omega_k^2 \left( q^k - \frac{c}{\omega_k^2} x \right)^2 \right], \quad (3.7)$$

where we have defined

$$\tilde{\omega}_{\text{r}}^2 = \omega_{\text{b}}^2 - c^2 \sum_{k=1}^{N_{\mathcal{E}}} \frac{1}{\omega_k^2}. \quad (3.8)$$

Since the harmonic oscillators  $q^k$  in the environment are expected to oscillate around the potential minimum  $cx/\omega_k^2$  when  $x$  varies slowly with time, the frequency  $\omega_{\text{b}}$  of the system  $\mathcal{S}$  is shifted to (3.8) due to the environment  $\mathcal{E}$  even at finite  $N_{\mathcal{E}}$ . Identifying  $\omega_{\text{r}}$  in (2.29) with  $\tilde{\omega}_{\text{r}}$  in (3.8) and using the frequency spectrum (3.4), we obtain the relationship between the coupling constant  $c$  at finite  $N_{\mathcal{E}}$  and the effective coupling  $\gamma$  as

$$c^2 = \frac{4\gamma}{\pi} \omega_{\text{cut}}^3 \left\{ \sum_{k=1}^{N_{\mathcal{E}}} \left( \frac{N_{\mathcal{E}}}{k} \right)^{2/3} \right\}^{-1}. \quad (3.9)$$

This is indeed consistent with the asymptotic behavior (3.6) at large  $N_{\mathcal{E}}$ .

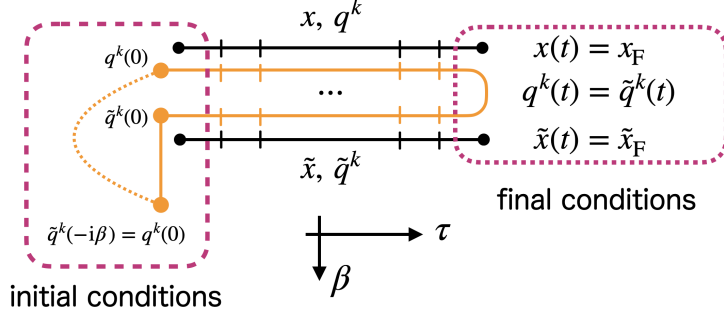


**Figure 1:** Schematic picture of the reduced density matrix of the system in the position space (3.14). The boundary conditions are imposed at the initial time and the final time.

### 3.2 The effective action for the Caldeira-Leggett model

In order to put the system on a computer, we discretize the time  $\tau$  as  $\tau_n = n\epsilon$  ( $n = 0, \dots, N_t$ ) and  $t \equiv \tau_{N_t}$ . Accordingly the variables  $x(\tau)$  and  $q_k(\tau)$  are also discretized as  $x_n = x(\tau_n)$  and  $q_n^k = q_k(\tau_n)$ . The action with the discretized time can be written as

$$S(x, q) = S_S(x) + S_{\mathcal{E}}(q) + S_{\text{int}}(x, q) , \quad (3.10)$$

$$S_S(x) = \frac{1}{2} \epsilon \sum_{n=0}^{N_t-1} \left[ \left( \frac{x_n - x_{n+1}}{\epsilon} \right)^2 - \omega_b^2 \frac{x_n^2 + x_{n+1}^2}{2} \right] , \quad (3.11)$$

$$S_{\mathcal{E}}(q) = \frac{1}{2} \epsilon \sum_{k=1}^{N_{\mathcal{E}}} \sum_{n=0}^{N_t-1} \left[ \left( \frac{q_n^k - q_{n+1}^k}{\epsilon} \right)^2 - \omega_k^2 \frac{(q_n^k)^2 + (q_{n+1}^k)^2}{2} \right] , \quad (3.12)$$

$$S_{\text{int}}(x, q) = c \epsilon \sum_{k=1}^{N_{\mathcal{E}}} \sum_{n=0}^{N_t-1} \frac{x_n q_n^k + x_{n+1} q_{n+1}^k}{2} . \quad (3.13)$$

The reduced density matrix of the system  $\mathcal{S}$  in the position basis can be given by

$$\rho_{\mathcal{S}}(x_F, \tilde{x}_F; t) = \int \mathcal{D}x \mathcal{D}\tilde{x} \left( \prod_{k=1}^{N_{\mathcal{E}}} \mathcal{D}q^k \mathcal{D}\tilde{q}^k \right) \rho_{\mathcal{S}}(x_0, \tilde{x}_0; 0) \left( \prod_{k=1}^{N_{\mathcal{E}}} \rho_{\mathcal{E}}^{(k)}(q_0^k, \tilde{q}_0^k, \beta) \right) e^{i(S(x, q) - S(\tilde{x}, \tilde{q}))} , \quad (3.14)$$

where the path integral measure is understood as the ordinary integration measure for discretized variables. At the final time, we impose  $x_{N_t} = x_F$ ,  $\tilde{x}_{N_t} = \tilde{x}_F$  corresponding to the element of the reduced density matrix to be calculated, and  $q_{N_t}^k = \tilde{q}_{N_t}^k$  corresponding to taking the trace with respect to the environment  $\mathcal{E}$  as in (2.14).

As the initial condition for the system  $\mathcal{S}$ , we consider a Gaussian wave packet<sup>6</sup>

$$\rho_{\mathcal{S}}(x, \tilde{x}; 0) = \psi_{\text{I}}(x) \psi_{\text{I}}^*(\tilde{x}) , \quad (3.15)$$

$$\psi_{\text{I}}(x) = \exp\left(-\frac{1}{4\sigma^2} x^2\right) . \quad (3.16)$$

<sup>6</sup>The following discussions can be easily generalized to the case with the initial wave function  $\psi_{\text{I}}(x) = \exp(-\frac{1}{4\sigma^2}(x - x_0)^2 + ipx)$  and to the case with two wave packets as we discuss in Section 5.

The initial condition of the environment  $\mathcal{E}$  is given by the canonical ensemble (2.5) with temperature  $T = \beta^{-1}$ . Here we introduce an additional path for the variables  $\tilde{q}^k$  in the imaginary time direction as depicted in Fig. 1 with the free Euclidean action<sup>7</sup>

$$S_0(\tilde{q}) = \frac{1}{2} \tilde{\epsilon} \sum_{k=1}^{N_{\mathcal{E}}} \sum_{j=0}^{N_{\beta}-1} \left[ \left( \frac{\tilde{q}_0^k(j+1) - \tilde{q}_0^k(j)}{\tilde{\epsilon}} \right)^2 + \omega_k^2 \frac{\tilde{q}_0^k(j+1)^2 + \tilde{q}_0^k(j)^2}{2} \right], \quad (3.17)$$

where we define  $\tilde{q}_0^k(j) \equiv \tilde{q}^k(-i(j\tilde{\epsilon}))$  and impose  $\tilde{q}_0^k = \tilde{q}_0^k(0)$  and  $q_0^k = \tilde{q}_0^k(N_{\beta})$  with the inverse temperature represented as  $\beta = N_{\beta} \tilde{\epsilon}$ .

To summarize, the reduced density matrix (3.14) of the system  $\mathcal{S}$  can be written as

$$\rho_{\mathcal{S}}(x_{\text{F}}, \tilde{x}_{\text{F}}; t) = \int \mathcal{D}x \mathcal{D}\tilde{x} \left( \prod_{k=1}^{N_{\mathcal{E}}} \mathcal{D}q^k \mathcal{D}\tilde{q}^k \mathcal{D}\tilde{q}_0^k \right) e^{-S_{\text{eff}}(x, \tilde{x}, q, \tilde{q}, \tilde{q}_0)}, \quad (3.18)$$

where the effective action is given by

$$S_{\text{eff}}(x, \tilde{x}, q, \tilde{q}, \tilde{q}_0) = -i \{S(x, q) - S(\tilde{x}, \tilde{q})\} + S_0(\tilde{q}_0) + \frac{1}{4\sigma^2} (x_0^2 + \tilde{x}_0^2). \quad (3.19)$$

Note that the first two terms are purely imaginary, whereas the last two terms are real. Since the integrand of (3.18) is complex, the sign problem occurs when one applies Monte Carlo methods naively.

### 3.3 Performing the path integral by the Gaussian integral

In the present case, the effective action (3.19) is quadratic with respect to the integration variables, and it can be written as

$$S_{\text{eff}}(x, \tilde{x}, q, \tilde{q}, \tilde{q}_0) = \frac{1}{2} X_{\mu} \mathcal{M}_{\mu\nu} X_{\nu} - C_{\mu} X_{\mu} + B, \quad (3.20)$$

where  $X_{\mu}$  ( $\mu = 1, \dots, D$ ) represents the integration variables collectively and the number of integration variables is  $D = 2N_t(1 + N_{\mathcal{E}}) + N_{\beta}N_{\mathcal{E}}$ . Note that  $\mathcal{M}$  is a  $D \times D$  complex symmetric matrix, which is independent of  $x_{\text{F}}$  and  $\tilde{x}_{\text{F}}$ , whereas  $C_{\mu}$  and  $B$  are defined by

$$\begin{aligned} C_{\mu} X_{\mu} &= -\frac{i}{\epsilon} (x_{\text{F}} x_{N_t-1} - \tilde{x}_{\text{F}} \tilde{x}_{N_t-1}) + \frac{i}{2} c \epsilon \sum_k (x_{\text{F}} - \tilde{x}_{\text{F}}) q_{N_t}^k, \\ B &= -\frac{i}{2} b (x_{\text{F}}^2 - \tilde{x}_{\text{F}}^2), \quad \text{where} \quad b = \frac{1}{\epsilon} - \frac{\omega_{\text{b}}^2 \epsilon}{2}. \end{aligned} \quad (3.21)$$

Since  $C_{\mu}$  is linear in  $x_{\text{F}}$  and  $\tilde{x}_{\text{F}}$ , let us write them as

$$C_{\mu} = i(c_{\mu} x_{\text{F}} - \tilde{c}_{\mu} \tilde{x}_{\text{F}}). \quad (3.22)$$

The saddle point of this effective action is given by

$$\bar{X}_{\mu} = \mathcal{M}_{\mu\nu}^{-1} C_{\nu}, \quad (3.23)$$

---

<sup>7</sup>This is actually not needed in the present case, where the initial density matrix is given explicitly by (2.5). Here we choose to do this in order to demonstrate that our formalism is useful also in more general cases, where the initial density matrix is not given explicitly.

and redefining the integration variables as  $Y_\mu = X_\mu - \bar{X}_\mu$ , the effective action becomes

$$S_{\text{eff}}(x, \tilde{x}, q, \tilde{q}, \tilde{q}_0) = \frac{1}{2} Y_\mu \mathcal{M}_{\mu\nu} Y_\nu + \left( B - \frac{1}{2} \bar{X}_\mu \mathcal{M}_{\mu\nu} \bar{X}_\nu \right) . \quad (3.24)$$

Integrating out  $Y_\mu$ , we obtain

$$\rho_S(x_F, \tilde{x}_F; t) = \frac{1}{\sqrt{\det \mathcal{M}}} e^{-\mathcal{A}} , \quad (3.25)$$

$$\begin{aligned} \mathcal{A} &= B - \frac{1}{2} \bar{X}_\mu \mathcal{M}_{\mu\nu} \bar{X}_\nu \\ &= B - \frac{1}{2} C_\mu (\mathcal{M}^{-1})_{\mu\nu} C_\nu \\ &= \frac{1}{2} \begin{pmatrix} x_F & \tilde{x}_F \end{pmatrix} \begin{pmatrix} -ib + c_\mu (\mathcal{M}^{-1})_{\mu\nu} c_\nu & -c_\mu (\mathcal{M}^{-1})_{\mu\nu} \tilde{c}_\nu \\ -\tilde{c}_\mu (\mathcal{M}^{-1})_{\mu\nu} c_\nu & ib + \tilde{c}_\mu (\mathcal{M}^{-1})_{\mu\nu} \tilde{c}_\nu \end{pmatrix} \begin{pmatrix} x_F \\ \tilde{x}_F \end{pmatrix} . \end{aligned} \quad (3.26)$$

Let us consider the magnitude  $|\rho_S(x_F, \tilde{x}_F; t)|$ , which is determined by

$$\begin{aligned} \text{Re} \mathcal{A} &= \frac{1}{2} \begin{pmatrix} x_F & \tilde{x}_F \end{pmatrix} \begin{pmatrix} J & -K \\ -K & J \end{pmatrix} \begin{pmatrix} x_F \\ \tilde{x}_F \end{pmatrix} \\ &= \frac{1}{4} \{ (J - K)(x_F + \tilde{x}_F)^2 + (J + K)(x_F - \tilde{x}_F)^2 \} , \end{aligned} \quad (3.27)$$

where we have defined

$$J = \text{Re}\{c_\mu (\mathcal{M}^{-1})_{\mu\nu} c_\nu\} = \text{Re}\{\tilde{c}_\mu (\mathcal{M}^{-1})_{\mu\nu} \tilde{c}_\nu\} , \quad (3.28)$$

$$K = \text{Re}\{c_\mu (\mathcal{M}^{-1})_{\mu\nu} \tilde{c}_\nu\} = \text{Re}\{\tilde{c}_\mu (\mathcal{M}^{-1})_{\mu\nu} c_\nu\} . \quad (3.29)$$

In order to investigate the decoherence, we define the quantities

$$\Gamma_{\text{diag}}(t) = 2(J - K) , \quad (3.30)$$

$$\Gamma_{\text{off-diag}}(t) = 2(J + K) , \quad (3.31)$$

which characterize the fall-off of the magnitude of the matrix element in the diagonal and off-diagonal directions, respectively, as

$$|\rho_S(x_F, \tilde{x}_F; t)| \simeq \exp \left\{ -\frac{1}{2} \Gamma_{\text{diag}}(t) \left( \frac{x_F + \tilde{x}_F}{2} \right)^2 - \frac{1}{2} \Gamma_{\text{off-diag}}(t) \left( \frac{x_F - \tilde{x}_F}{2} \right)^2 \right\} , \quad (3.32)$$

omitting the prefactor independent of  $x_F$  and  $\tilde{x}_F$ . From (2.38), we expect the behavior<sup>8</sup>

$$\Gamma_{\text{off-diag}}(t) \sim \frac{16\gamma}{\beta} t , \quad (3.33)$$

which enables us to probe the decoherence at high temperature.

---

<sup>8</sup>This equation corresponds to Eq. (29) in the letter version [42] of this work, where we had 8 instead of 16 by mistake. This affects the prediction from the master equation by a factor of 2 in subsequent discussions in Ref. [42] although the main conclusion of that paper remains the same. This correction is crucial in the agreement with the prediction observed in Section 4.3.

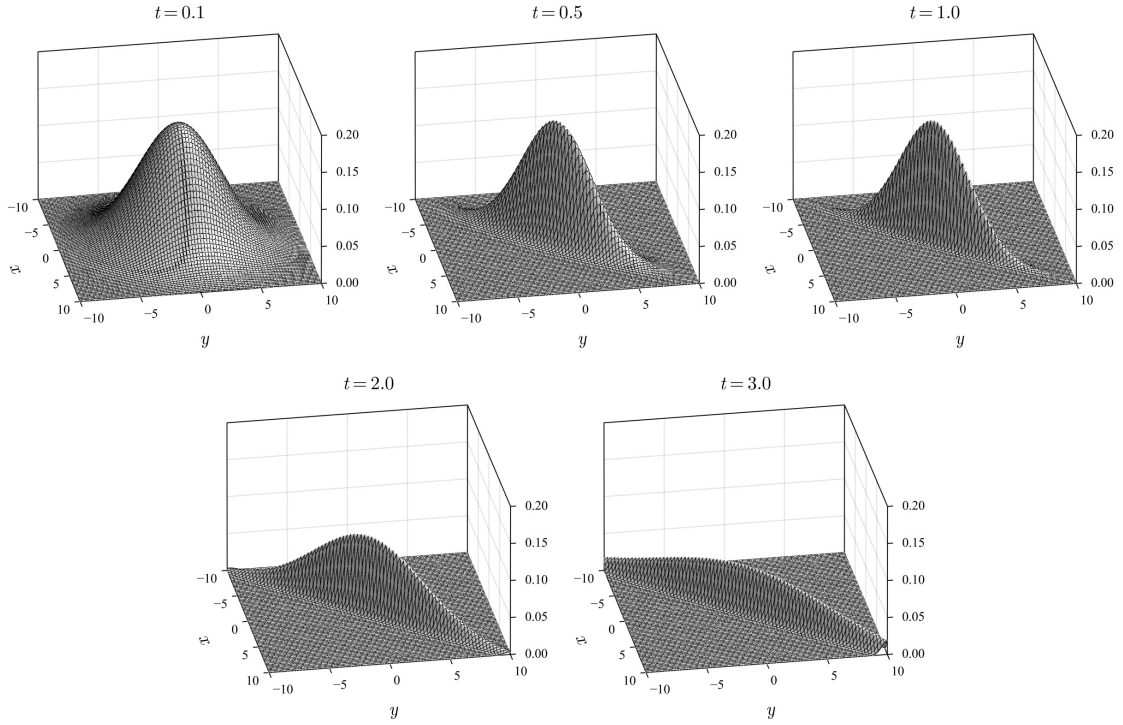


**Figure 2:** The reduced density matrix  $|\rho_S(x, y; t)|$  is plotted in the  $xy$  plane for  $t = 0.1, 0.5, 1.0, 2.0, 3.0$  with  $N_{\mathcal{E}} = 64$ ,  $\beta = 0.05$ ,  $\gamma = 0.1$  and  $\omega_{\text{cut}} = 2$ .

#### 4 Numerical results for a single wave packet

In this section we consider the case in which the initial wave function of the system  $\mathcal{S}$  is assumed to be the ground state of the harmonic oscillator with the renormalized frequency  $\omega_r$ , which corresponds to (3.16) with  $\sigma^2 = \frac{1}{2\omega_r^2}$ . Throughout this section, we set<sup>9</sup>  $\omega_r = 0.08$ . The lattice spacing in the time direction is chosen to be  $\epsilon = 0.05$ , whereas the lattice spacing in the temperature direction is chosen to be  $\tilde{\epsilon} = 0.05$  for  $\beta \geq 0.2$ , and  $\tilde{\epsilon} = \beta/4$  for  $\beta \leq 0.2$ . In Appendix A, we present some evidence that changing the lattice spacing does not alter our main conclusion.

In Fig. 2, we plot the behavior of the reduced density matrix (3.32) for  $N_{\mathcal{E}} = 64$ ,  $\beta = 0.05$ ,  $\gamma = 0.1$  and  $\omega_{\text{cut}} = 2$ , which satisfy the hierarchy  $\omega_r \ll \omega_{\text{cut}} \ll \beta^{-1} = T$  required in deriving the master equation. Here the reduced density matrix  $\rho_S(x, y; t)$  is correctly normalized by the factor  $\sqrt{2\pi/\Gamma_{\text{diag}}(t)}$ . At  $t = 0$ , the Gaussian distribution is symmetric since  $\Gamma_{\text{diag}}(0) = \Gamma_{\text{off-diag}}(0) = 2\omega_r$ . Up to  $t \simeq 1$ , the diagonal elements do not change much while the off-diagonal elements decrease with  $t$ , which clearly indicates the effect of decoherence. In order to investigate it more quantitatively, we discuss the time evolution of  $\Gamma_{\text{diag}}(t)$  and  $\Gamma_{\text{off-diag}}(t)$  for various  $N_{\mathcal{E}}$ ,  $\beta$ ,  $\gamma$  and  $\omega_{\text{cut}}$  in what follows.

<sup>9</sup>The bare frequency  $\omega_b$  is determined by (2.29), whereas the coupling constant  $c$  is determined by (3.9).

#### 4.1 Increasing the number of harmonic oscillators

Let us first present our results for increasing  $N_{\mathcal{E}}$ , the number of harmonic oscillators in the environment  $\mathcal{E}$ . In Fig. 3 we plot  $\Gamma_{\text{diag}}(t)$  and  $\Gamma_{\text{off-diag}}(t)$  for various  $N_{\mathcal{E}}$  with  $\beta = 0.05$ ,  $\gamma = 0.1$  and  $\omega_{\text{cut}} = 2$ . We see a clear converging behavior to  $N_{\mathcal{E}} = \infty$  for  $t \lesssim 3$ .

In Fig. 4 we plot  $\Gamma_{\text{off-diag}}(t)$  (Left) and  $\Gamma_{\text{diag}}(t)$  (Right) against  $1/N_{\mathcal{E}}$  for various  $t$ . We find that our data for the chosen values of  $t$  can be nicely fitted to quadratic functions at sufficiently large  $N_{\mathcal{E}}$ , which enables us to extrapolate our data to  $N_{\mathcal{E}} = \infty$  as represented by the inverted triangles. This confirms the validity of our choice (3.9) of the coupling constant  $c$  for finite  $N_{\mathcal{E}}$ .

The linear growth of  $\Gamma_{\text{off-diag}}(t)$  appears after  $t = 0.2$ , which is consistent with the typical time scale of the decoherence  $\tau_d = \frac{\beta}{2\gamma} = 0.25$ , and continues until  $t \sim 1$ , where  $\Gamma_{\text{diag}}(t)$  start to decrease rapidly, indicating that the effects of the environment other than decoherence are coming into play. The dotted line in Fig. 3 (Top-Left) and (Bottom) represents a fit of our data in the region  $0.4 \leq t \leq 1.1$  to the behavior  $A \frac{16\gamma}{\beta} t + B$  yielding  $A \sim 0.69$ , which is smaller than the predicted value 1. In fact, the fitted value of  $A$  increases toward the predicted value with increasing  $\omega_{\text{cut}}$  as we will see in Section 4.3.

From Fig. 3 (Top-Right), we find that  $\Gamma_{\text{diag}}(t)$  becomes constant at late times, which may be interpreted as thermalization since the environment can be regarded as a thermal bath with the inverse temperature  $\beta$  in the  $N_{\mathcal{E}} \rightarrow \infty$  limit. If so, it is expected that the reduced density matrix  $\rho_S(x, \tilde{x}, t)$  approaches

$$\lim_{t \rightarrow \infty} \rho_S(x, \tilde{x}, t) = \sqrt{\frac{\omega_r}{2\pi \sinh \beta \omega_r}} \exp \left[ -\frac{\omega_r}{2 \sinh \beta \omega_r} \{ (x^2 + \tilde{x}^2) \cosh \beta \omega_r - 2x\tilde{x} \} \right] \quad (4.1)$$

similarly to (2.6). In particular, it is expected that

$$\lim_{t \rightarrow \infty} \Gamma_{\text{diag}}(t) = 2\omega_r \tanh \frac{\beta \omega_r}{2}, \quad \lim_{t \rightarrow \infty} \Gamma_{\text{off-diag}}(t) = 2\omega_r \coth \frac{\beta \omega_r}{2}. \quad (4.2)$$

In Fig. 5, we plot the large- $N_{\mathcal{E}}$  extrapolated results for  $\Gamma_{\text{diag}}(t)$  against time, which are consistent with the behavior  $2\omega_r \tanh \frac{\beta \omega_r}{2} + A \exp(-Bt)$ .

On the other hand, the off-diagonal part shown in Fig. 3 (Top-Left) has significant  $N_{\mathcal{E}}$  dependence at late times. This may be due to the recurrence for a finite environment. (For similar discussions, see Section 2.10 of Ref. [1] and references therein.) According to (4.2),  $\Gamma_{\text{off-diag}}(t)$  is expected to approach  $2\omega_r \coth \frac{\beta \omega_r}{2} \approx 80$  at late times for sufficiently large  $N_{\mathcal{E}}$ . In order to confirm this we need to increase  $N_{\mathcal{E}}$  and the time  $t$  further, which we leave for future investigations.

Here let us comment on the computational efforts required for such an analysis. To compute the reduced density matrix at each  $t$ , we solve the equation (3.23) numerically by the LU decomposition, whose cost scales as  $O(D^3)$  for the matrix size  $D = 2N_t(1 + N_{\mathcal{E}}) + N_{\beta}N_{\mathcal{E}}$ . In order to add another data point with increased time  $t = N_t \epsilon$  for fixed  $\epsilon$ , we need the computational time of  $O(N_t^3)$  since  $D = O(N_t)$ . In order to obtain results for larger  $N_{\mathcal{E}}$ , we need the computational time of  $O(N_{\mathcal{E}}^3)$  since  $D = O(N_{\mathcal{E}})$ . Therefore, taking both limits  $N_{\mathcal{E}} \rightarrow \infty$  and  $t \rightarrow \infty$  seems to be a big challenge.



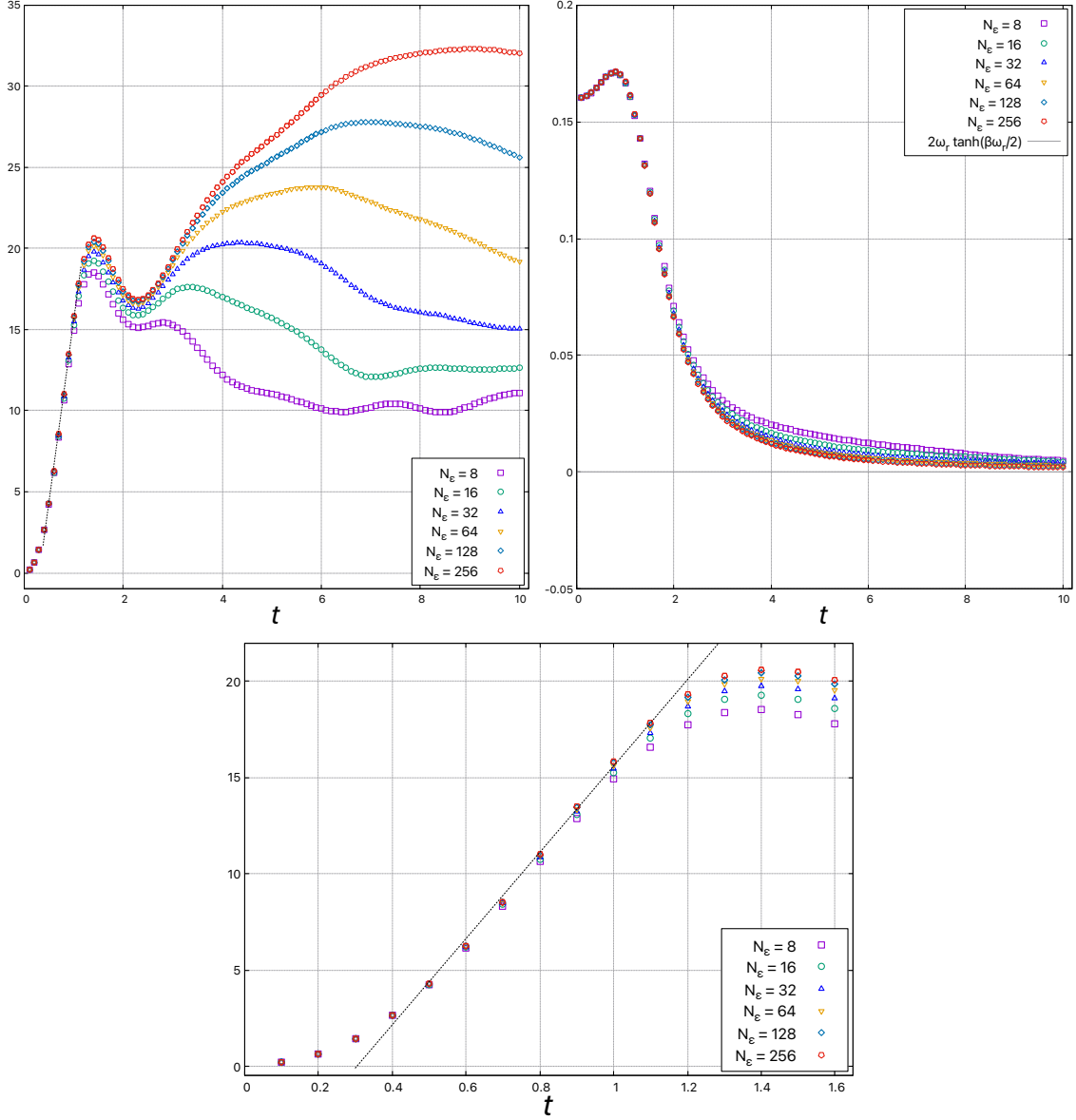


**Figure 3:** The quantities  $\Gamma_{\text{off-diag}}(t)$  (Top-Left) and  $\Gamma_{\text{diag}}(t)$  (Top-Right) are plotted against  $t$  for  $N_E = 8, 16, \dots, 256$  with  $\beta = 0.05$ ,  $\gamma = 0.1$  and  $\omega_{\text{cut}} = 2$ . In the Top-Left panel, the dotted line represents a fit of the  $N_E = 256$  data within the region  $0.4 \leq t \leq 1.1$  to the behavior  $A \frac{16\gamma}{\beta} t + B$ . In the Top-Right panel, the solid gray line represents  $\frac{1}{x_F} \frac{\partial}{\partial x_F} \log \rho_{\text{thermal}}(x_F, -x_F; \beta)$ , which is the value expected to be approached at  $t \rightarrow \infty$ . (Bottom) A zoom-in of the Top-Left panel, where we present  $\Gamma_{\text{off-diag}}(t)$  for  $t \leq 1.6$ .

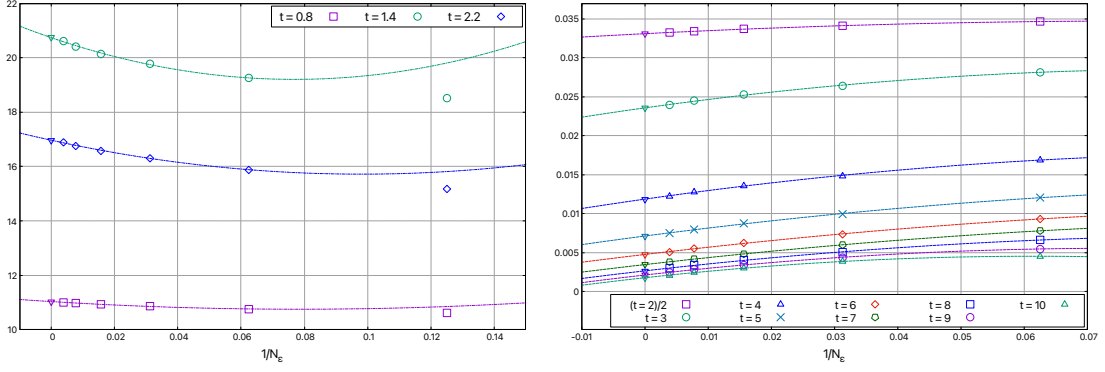


**Figure 4:** (Left) The quantity  $\Gamma_{\text{off-diag}}(t)$  is plotted against  $1/N_{\mathcal{E}}$  at  $t = 0.8, 1.4, 2.2$ . (Right) The quantity  $\Gamma_{\text{diag}}(t)$  is plotted against  $1/N_{\mathcal{E}}$  at  $t = 2, 3, \dots, 10$ . The results for  $t = 2$  are divided by 2 for the sake of visualization. In both panels, the lines represent quadratic fits to our data at large  $N_{\mathcal{E}}$  and the inverted triangles represent the extrapolated values at  $N_{\mathcal{E}} = \infty$ .

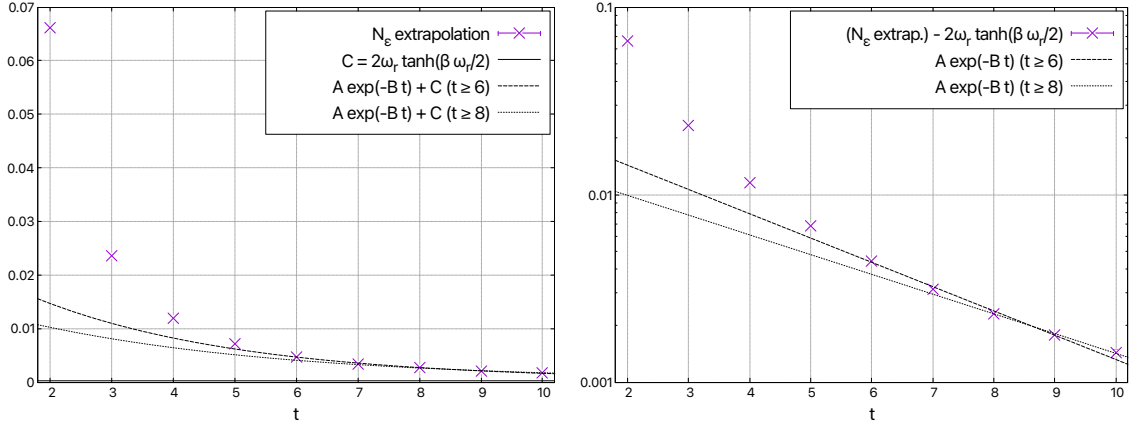


**Figure 5:** (Left) The large- $N_{\mathcal{E}}$  extrapolated results for  $\Gamma_{\text{diag}}(t)$  at  $t = 2, 3, \dots, 10$  obtained from Fig. 4 are plotted as a function of  $t$ . The horizontal solid line represents the value  $C_{\text{th}} = 2\omega_r \tanh(\beta \omega_r/2) = 0.00032$  predicted by thermalization at the inverse temperature  $\beta = 0.05$ , whereas the dashed line and the dotted line represent fits to  $C_{\text{th}} + A \exp(-Bt)$  with the fitting range  $t \geq 6$  and  $t \geq 8$ , respectively. (Right) The deviation of  $\Gamma_{\text{diag}}(t)$  from the predicted value  $C_{\text{th}}$  is plotted against  $t$  in the log scale. The dashed line and the dotted line represent linear fits to the data for  $t \geq 6$  and  $t \geq 8$ , respectively.

## 4.2 Dependence on the coupling and the temperature

Next we discuss how our results depend on the coupling  $\gamma$  and the temperature. In Fig. 6, we plot  $\Gamma_{\text{off-diag}}(t)$  (Top-Left) and  $\Gamma_{\text{diag}}(t)$  (Top-Right) against  $t$  for  $\gamma = 0.025, 0.05, \dots, 0.4$  with  $N_{\mathcal{E}} = 64$ ,  $\beta = 0.05$  and  $\omega_{\text{cut}} = 2$  fixed. We observe a linear growth of  $\Gamma_{\text{off-diag}}(t)$  from

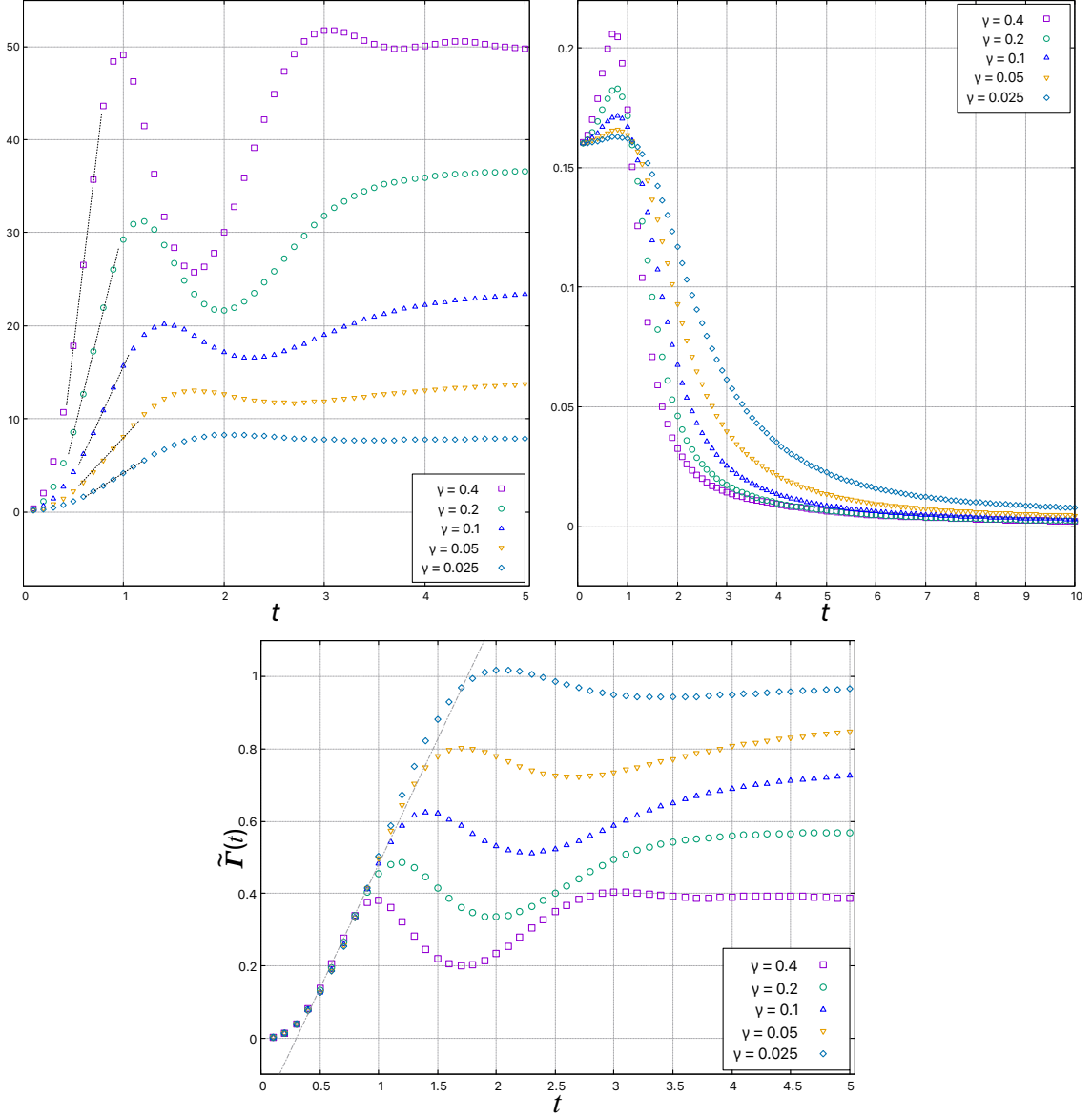


**Figure 6:** The quantities  $\Gamma_{\text{off-diag}}(t)$  (Top-Left) and  $\Gamma_{\text{diag}}(t)$  (Top-Right) are plotted against  $t$  for  $\gamma = 0.025, 0.05, \dots, 0.4$  with  $N_{\mathcal{E}} = 64$ ,  $\beta = 0.05$  and  $\omega_{\text{cut}} = 2$  fixed. The dotted lines in the Top-Left panel represent fits to the behavior  $A \frac{16\gamma}{\beta} t + B$  at early times. (Bottom) The rescaled quantity  $\tilde{\Gamma}(t)$  defined by (4.3) is plotted against  $t$ , which reveals a clear scaling behavior. The dash-dotted line represents a fit of the  $\gamma = 0.1$  data within  $0.6 \leq t \leq 1$  to a linear behavior  $At + B$ , where  $A \sim 0.69$  is obtained.

$t \approx 0.5$ . In the bottom panel, we plot the rescaled quantity

$$\tilde{\Gamma}(t) = \frac{\beta}{16\gamma} \{ \Gamma_{\text{off-diag}}(t) - \Gamma_{\text{off-diag}}(0) \}, \quad (4.3)$$

which reveals a clear scaling behavior at early times. While the scaling behavior implies  $\Gamma_{\text{off-diag}}(t) \sim A \frac{16\gamma}{\beta} t$ , which is qualitatively consistent with the prediction from the master

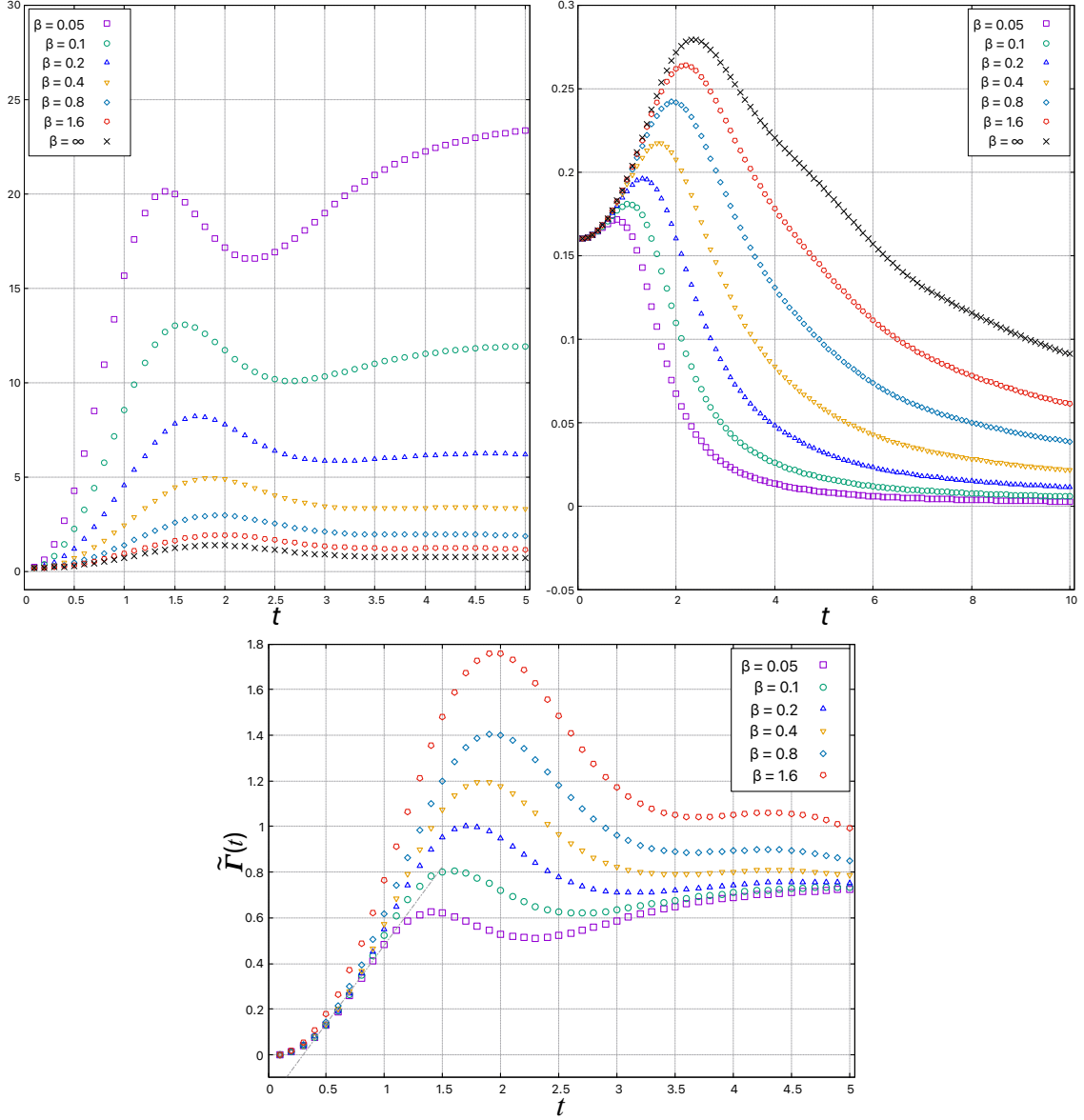


**Figure 7:** The quantities  $\Gamma_{\text{off-diag}}(t)$  (Top-Left) and  $\Gamma_{\text{diag}}(t)$  (Top-Right) are plotted for  $\beta = 0.05, 0.1, 0.2, 0.4, 0.8, 1.6$  and  $\infty$  with  $N_{\mathcal{E}} = 64$ ,  $\gamma = 0.1$  and  $\omega_{\text{cut}} = 2$  fixed. (Bottom) The rescaled quantity  $\tilde{\Gamma}(t)$  defined by (4.3) is plotted against  $t$ , which reveals a clear scaling behavior at small  $\beta$ . The dash-dotted line represents a fit of the  $\beta = 0.05$  data within  $0.4 \leq t \leq 1.1$  to a linear behavior  $At + B$ , where  $A \sim 0.69$  is obtained.

equation, the coefficient is  $A \sim 0.69$ , which is smaller than the predicted value 1. At  $\gamma = 0.05$ , we start to see a deviation from a linear behavior, which is understandable since  $\gamma/\beta \gg 1$  is required to justify the approximation of the master equation by (2.37).

In Fig. 7, we plot  $\Gamma_{\text{off-diag}}(t)$  (Top-Left) and  $\Gamma_{\text{diag}}(t)$  (Top-Right) against  $t$  for  $\beta = 0.05, 0.1, 0.2, 0.4, 0.8, 1.6$  and  $\infty$ <sup>10</sup> with  $N_{\mathcal{E}} = 64$ ,  $\gamma = 0.1$  and  $\omega_{\text{cut}} = 2$ . In the bottom panel,

<sup>10</sup>In order to obtain the results at zero temperature, which corresponds to  $\beta = \infty$ , we have performed

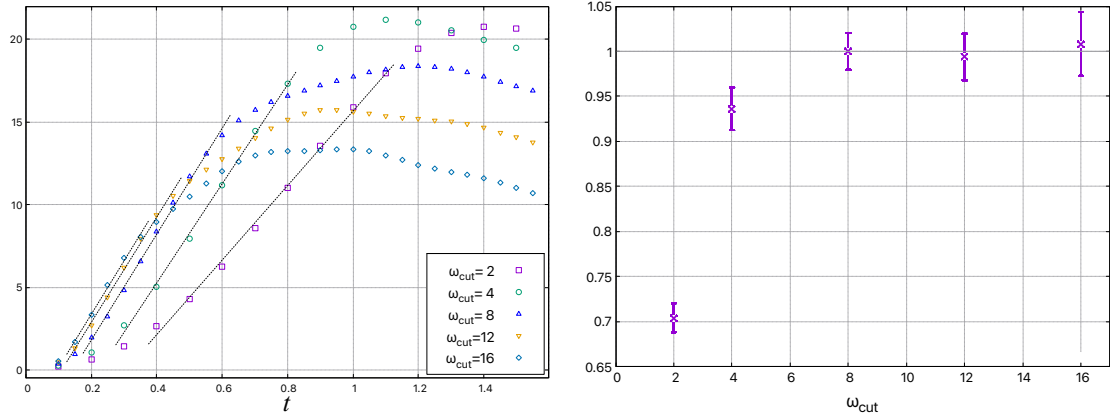


**Figure 8:** (Left) The quantity  $\Gamma_{\text{off-diag}}(t)$  is plotted for various  $\omega_{\text{cut}}$  with  $N_{\mathcal{E}} = 512$ ,  $\beta = 0.05$  and  $\gamma = 0.1$ . The dotted and dashed lines represent the fit of data at early times to a linear behavior  $A \frac{16\gamma}{\beta} t + B$ . (Right) The coefficient  $A$  obtained by the linear fit is plotted against  $\omega_{\text{cut}}$ . The error bars represent the fitting errors.

we plot the rescaled quantity (4.3), which shows the emergence of a clear scaling behavior at early times as  $\beta$  is decreased. At lower temperature, we see clear deviation from the scaling behavior predicted by the master equation, which assumes both  $\beta\omega_{\text{cut}} \ll 1$  (See (2.30).) and  $\gamma/\beta \gg 1$ .

### 4.3 Dependence on the cutoff frequency $\omega_{\text{cut}}$

So far, we have confirmed the linear growth for  $\Gamma_{\text{off-diag}}(t)$  at early times with a slope proportional to  $\gamma/\beta$  as predicted by the CL master equation. However, the slope was smaller than the predicted value by 30%. In this section, we show that the numerical coefficient increases toward the predicted value as we increase  $\omega_{\text{cut}}$ .

In Fig. 8 (Left), we plot  $\Gamma_{\text{off-diag}}(t)$  up to  $t = 1.6$  for  $\omega_{\text{cut}} = 2, 4, 8, 12, 16$  with  $N_{\mathcal{E}} = 512$ ,  $\beta = 0.05$  and  $\gamma = 0.1$ . We have used a larger value for  $N_{\mathcal{E}}$  in order to keep the frequencies (3.4) in the environment dense enough. (See appendix A for more details.) We fit our data to a linear behavior  $A \frac{16\gamma}{\beta} t + B$  for each  $\omega_{\text{cut}}$ . In Fig. 8 (Right), we plot the coefficient  $A$  obtained by the fits as a function of  $\omega_{\text{cut}}$ , where the error bars represent the fitting errors. We find good agreement with the predicted value  $A = 1$  for  $\omega_{\text{cut}} = 8, 12, 16$ . This is understandable in view of the condition<sup>11</sup>  $\omega_{\text{cut}} \gg \omega_r = 0.08$ , which is used to approximate the function  $f(\tau)$  in (2.27) by the delta function.

---

an independent calculation by replacing the closed imaginary-time path for  $\mathcal{E}$  with the ground-state wave function  $\psi_{\text{init}}(q) = e^{-\sum_k \frac{1}{2} \omega_k (q_k)^2}$ . As  $\beta$  is increased in Fig. 7 (Top), our results approach smoothly to the result at  $\beta = \infty$  obtained in this way.

<sup>11</sup>Note, however, that the condition  $\omega_{\text{cut}} \ll \beta^{-1} = 20$  is not well satisfied for  $\omega_{\text{cut}} = 8, 12, 16$ , which suggests that the condition  $\omega_{\text{cut}} \gg \omega_r$  is more important for the agreement with the prediction  $A = 1$ .

## 5 Numerical results for the “double-slit experiment”

In this section, we generalize our calculations to the initial state with two wave packets, which was studied also in Refs. [36, 38, 39, 50]. This enables us, in particular, to investigate the decoherence through the interference terms in the reduced density matrix analogously to the situation in the well-known double-slit experiment. We will see the effect of decoherence clearly as the fading of the interference pattern.

### 5.1 Extending the calculations to two wave packets

Here we discuss how one can extend the calculations in Section 3 to the case of two wave packets. Let us consider the initial wave function

$$\begin{aligned}\psi_I(x) &= \psi_0(x) + \psi_1(x) , \\ \psi_0(x) &= \exp\left(-\frac{1}{4\sigma^2}(x - \xi)^2 - ipx\right) , \\ \psi_1(x) &= \exp\left(-\frac{1}{4\sigma^2}(x + \xi)^2 + ipx\right) ,\end{aligned}\tag{5.1}$$

where  $\psi_0(x)$  and  $\psi_1(x)$  represent the wave packets that pass through the “double slit” separated by some distance  $2\xi > 0$  and move towards  $x = 0$  with some momentum  $p > 0$ . The corresponding reduced density matrix of the system (3.15) can be decomposed as

$$\rho_S(x, \tilde{x}; t = 0) = \sum_{a,b=0}^1 \rho_{ab}(x, \tilde{x}; t = 0) ,\tag{5.2}$$

$$\rho_{ab}(x, \tilde{x}; t = 0) = \psi_a(x) \psi_b^*(\tilde{x}) .\tag{5.3}$$

Plugging this in (3.14), we obtain the time-evolved reduced density matrix

$$\rho_S(x, \tilde{x}; t) = \sum_{a,b=0}^1 \rho_{ab}(x, \tilde{x}; t) ,\tag{5.4}$$

where  $\rho_{ab}(x, \tilde{x}; t)$  is given by

$$\rho_{ab}(x_F, \tilde{x}_F; t) = \int \mathcal{D}x \mathcal{D}\tilde{x} \left( \prod_{k=1}^{N_E} \mathcal{D}q^k \mathcal{D}\tilde{q}^k \mathcal{D}\tilde{q}_0^k \right) e^{-S_{ab}(x, \tilde{x}, q, \tilde{q}, \tilde{q}_0)} ,\tag{5.5}$$

with the effective action  $S_{ab}$  given by

$$\begin{aligned}S_{ab}(x, \tilde{x}, q, \tilde{q}, \tilde{q}_0) &= -i \{S(x, q) - S(\tilde{x}, \tilde{q})\} + S_0(\tilde{q}_0) \\ &\quad + \frac{1}{4\sigma^2} \left\{ x_0 - (-1)^a \xi \right\}^2 + i(-1)^a p x_0 + \frac{1}{4\sigma^2} \left\{ \tilde{x}_0 - (-1)^b \xi \right\}^2 - i(-1)^b p \tilde{x}_0 .\end{aligned}\tag{5.6}$$

Similarly to (3.20), the effective action can be written as

$$S_{ab}(x, \tilde{x}, q, \tilde{q}, \tilde{q}_0) = \frac{1}{2} X_\mu \mathcal{M}_{\mu\nu} X_\nu - (C_\mu + E_\mu^{ab}) X_\mu + \left( B + \frac{1}{2\sigma^2} \xi^2 \right) ,\tag{5.7}$$

$$E_\mu^{ab} = (-1)^a (k - ip) e_\mu + (-1)^b (k + ip) \tilde{e}_\mu ,\tag{5.8}$$

where  $k = \frac{\xi}{2\sigma^2}$  and the unit vectors  $e_\mu$  and  $\tilde{e}_\mu$  are defined by  $x_0 = e_\mu X_\mu$  and  $\tilde{x}_0 = \tilde{e}_\mu X_\mu$ .

The saddle point of the action (5.7) is given by

$$\bar{X}_\mu^{ab} = \mathcal{M}_{\mu\nu}^{-1} (C_\nu + E_\nu^{ab}) , \quad (5.9)$$

and we obtain each component of the reduced density matrix as

$$\rho_{ab}(x_F, \tilde{x}_F; t) = \frac{1}{\sqrt{\det \mathcal{M}}} e^{-\mathcal{A}_{ab} - \frac{1}{2\sigma^2} \xi^2} , \quad (5.10)$$

$$\begin{aligned} \mathcal{A}_{ab} &= B - \frac{1}{2} \bar{X}_\mu^{ab} \mathcal{M}_{\mu\nu} \bar{X}_\nu^{ab} \\ &= B - \frac{1}{2} (C_\mu + E_\mu^{ab}) (\mathcal{M}^{-1})_{\mu\nu} (C_\nu + E_\nu^{ab}) \\ &= \frac{1}{2} \begin{pmatrix} x_F & \tilde{x}_F \end{pmatrix} \begin{pmatrix} -i b + c_\mu (\mathcal{M}^{-1})_{\mu\nu} c_\nu & -c_\mu (\mathcal{M}^{-1})_{\mu\nu} \tilde{c}_\nu \\ -\tilde{c}_\mu (\mathcal{M}^{-1})_{\mu\nu} c_\nu & i b + \tilde{c}_\mu (\mathcal{M}^{-1})_{\mu\nu} \tilde{c}_\nu \end{pmatrix} \begin{pmatrix} x_F \\ \tilde{x}_F \end{pmatrix} \\ &\quad - i E_\mu^{ab} (\mathcal{M}^{-1})_{\mu\nu} (c_\nu x_F - \tilde{c}_\nu \tilde{x}_F) - \frac{1}{2} E_\mu^{ab} (\mathcal{M}^{-1})_{\mu\nu} E_\nu^{ab} . \end{aligned} \quad (5.11)$$

Note that there are relationships between the components as

$$\rho_{00}(x_F, \tilde{x}_F; t) = \rho_{11}(-x_F, -\tilde{x}_F; t) , \quad (5.12)$$

$$\rho_{01}(x_F, \tilde{x}_F; t) = \rho_{10}(-x_F, -\tilde{x}_F; t) , \quad (5.13)$$

due to the symmetry  $x \mapsto -x$  of our chosen setup.

Here we focus on the diagonal elements of the density matrix<sup>12</sup> corresponding to  $x_F = \tilde{x}_F = x$ , for which the exponent  $\mathcal{A}_{ab}$  reduces to

$$\mathcal{A}_{ab} = \frac{1}{2} (c_\mu - \tilde{c}_\mu) (\mathcal{M}^{-1})_{\mu\nu} (c_\nu - \tilde{c}_\nu) x^2 - i E_\mu^{ab} (\mathcal{M}^{-1})_{\mu\nu} (c_\nu - \tilde{c}_\nu) x - \frac{1}{2} E_\mu^{ab} (\mathcal{M}^{-1})_{\mu\nu} E_\nu^{ab} . \quad (5.14)$$

Thus each component of the density matrix is given by

$$\rho_{00}(x, x; t) \simeq \exp \left\{ -\frac{1}{2} K_1 x^2 - (k K_2 - p K_3) x + \frac{1}{2} (k^2 K_4 - p^2 K_5) \right\} , \quad (5.15)$$

$$\rho_{11}(x, x; t) = \rho_{00}(-x, -x; t) , \quad (5.16)$$

$$\rho_{01}(x, x; t) \simeq \exp \left\{ -\frac{1}{2} K_1 x^2 + i (k K_3 + p K_2) x + \frac{1}{2} (k^2 K_5 - p^2 K_4) \right\} , \quad (5.17)$$

$$\rho_{10}(x, x; t) = \rho_{01}(-x, -x; t) , \quad (5.18)$$

omitting the prefactors common to all components. The real quantities  $K_i$  ( $i = 1, \dots, 5$ ) are defined as

$$K_1 = (c_\mu - \tilde{c}_\mu) \operatorname{Re}(\mathcal{M}^{-1})_{\mu\nu} (c_\nu - \tilde{c}_\nu) , \quad (5.19)$$

$$K_2 = (e_\mu + \tilde{e}_\mu) \operatorname{Im}(\mathcal{M}^{-1})_{\mu\nu} (c_\nu - \tilde{c}_\nu) , \quad (5.20)$$

$$K_3 = (e_\mu - \tilde{e}_\mu) \operatorname{Re}(\mathcal{M}^{-1})_{\mu\nu} (c_\nu - \tilde{c}_\nu) , \quad (5.21)$$

$$K_4 = (e_\mu + \tilde{e}_\mu) \operatorname{Re}(\mathcal{M}^{-1})_{\mu\nu} (e_\nu + \tilde{e}_\nu) , \quad (5.22)$$

$$K_5 = (e_\mu - \tilde{e}_\mu) \operatorname{Re}(\mathcal{M}^{-1})_{\mu\nu} (e_\nu - \tilde{e}_\nu) . \quad (5.23)$$

---

<sup>12</sup>See Appendix B for the discussions on the off-diagonal elements of the density matrix.

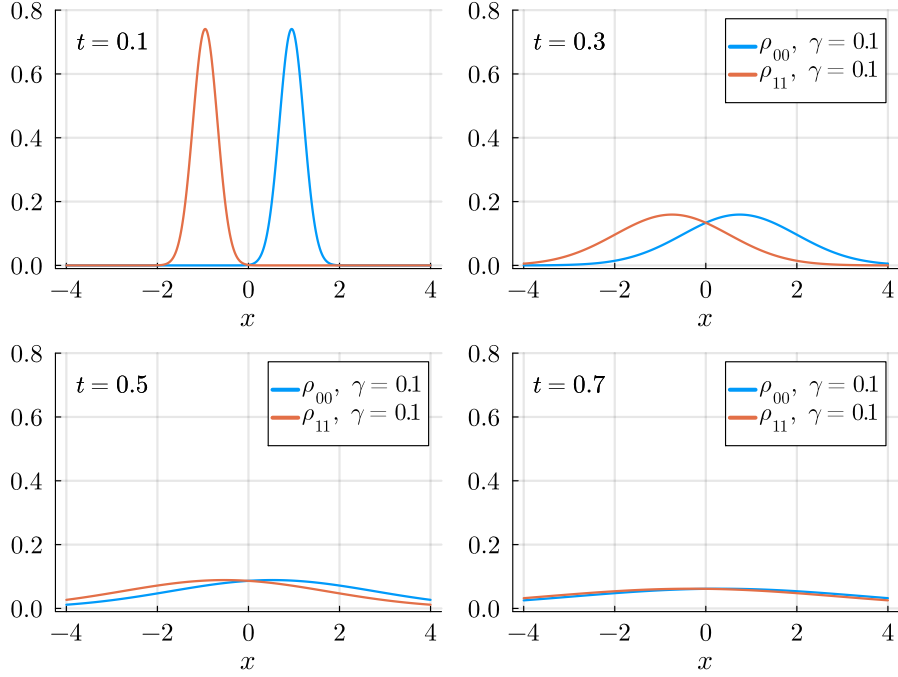


**Figure 9:** The direct terms  $\rho_{00}(x, x; t)$  and  $\rho_{11}(x, x; t)$  are plotted against  $x$  for  $t = 0.1, 0.3, 0.5, 0.7$  with  $\gamma = 0.1$ .

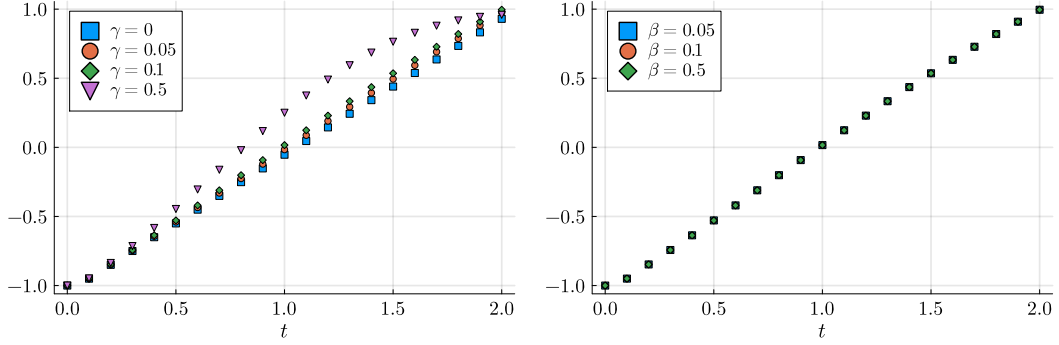


**Figure 10:** The peak position of  $\rho_{00}(x, x; t)$  is plotted for various  $\gamma$  with  $\beta = 0.05$  (Left) and for various  $\beta$  with  $\gamma = 0.1$  (Right).

In fact, we need to normalize the reduced density matrix as  $\rho_{ab}(x, \tilde{x}; t) \mapsto \frac{1}{\mathcal{N}} \rho_{ab}(x, \tilde{x}; t)$  with the normalization factor defined by

$$\mathcal{N}(t) = \int dx \rho_S(x, x; t) = 2\sqrt{\frac{2\pi}{K_1}} \left[ \exp \left\{ \frac{1}{2} \frac{(kK_2 - pK_3)^2}{K_1} + \frac{1}{2} (k^2 K_4 - p^2 K_5) \right\} + \exp \left\{ -\frac{1}{2} \frac{(kK_3 + pK_2)^2}{K_1} + \frac{1}{2} (k^2 K_5 - p^2 K_4) \right\} \right]. \quad (5.24)$$

In what follows, we assume that the reduced density matrix is normalized in this way.



## 5.2 The effect of decoherence on the interference pattern

Here we present our results for the time-evolved reduced density matrix obtained in the way described in the previous section. Throughout this section, we set the parameters as  $N_{\mathcal{E}} = 64$ ,  $\omega_{\text{cut}} = 2$ ,  $\omega_r = 0$ ,  $\sigma = 0.1$ ,  $\xi = 1$ ,  $p = 1$ . Note also that  $k = \xi/(2\sigma^2) = 1/(2 \times 0.1^2) = 50$ . The lattice spacing in the time direction is chosen to be  $\epsilon = 0.05$ , whereas the lattice spacing in the temperature direction is chosen to be  $\tilde{\epsilon} = 0.0125$ .

Let us first discuss the direct terms  $\rho_{00}(x, x; t)$  and  $\rho_{11}(x, x; t)$  in the reduced density matrix, which represent the contribution from  $\psi_0(x)$  and  $\psi_1(x)$ , respectively. In Fig. 9, we plot these quantities against  $x$  for  $t = 0.1, 0.3, 0.5, 0.7$ . We find that they are given by two Gaussian distributions, which are peaked around  $x = 1$  and  $x = -1$ , respectively, at early times, and come close to each other with time due to the chosen initial condition (5.1). The results obtained here are actually quite close to those for  $\gamma = 0$ . This implies that the direct terms  $\rho_{00}(x, x; t)$  and  $\rho_{11}(x, x; t)$  are not sensitive to the interaction with the environment at least for  $\gamma \lesssim 0.1$ .

In Fig. 10, we plot the peak position of  $\rho_{00}(x, x; t)$ , which is given by  $\frac{kK_2 - pK_3}{K_1}$  from (5.15), against  $t$ . Note that the time dependence of the peak position should agree with the classical motion of free particles for  $\gamma = 0$  due to our choice  $\omega_r = 0$ . From our results for  $\gamma > 0$ , there seems to be some “effective  $\omega_r$ ” induced by the interactions with the environment on top of the expected deceleration due to the friction-like effects. On the other hand, we do not see clear  $\beta$  dependence for a fixed  $\gamma$ .

Next we consider the interference terms

$$\rho_{01}(x, x; t) + \rho_{10}(x, x; t) = 2 \text{Re } \rho_{01}(x, x; t) . \quad (5.25)$$

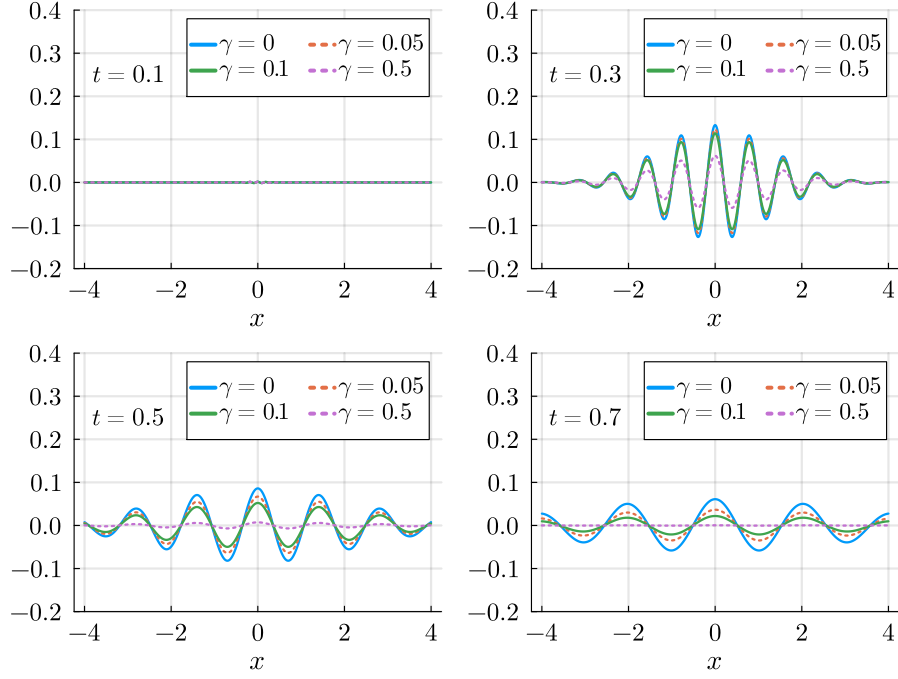
In Fig. 11, we plot  $\text{Re } \rho_{01}(x, x; t)$  for various  $\gamma$  with fixed  $\beta = 0.05$  (a) and for various  $\beta$  with fixed  $\gamma = 0.1$  (b). We find that the amplitude of the oscillation gets smaller as  $\gamma/\beta$  increases. In Fig. 11 (b), the result for  $\beta = 0.5$  with  $\gamma = 0.1$  is almost identical to the result for  $\gamma = 0$ , which is shown for comparison.

In order to clarify the effect of decoherence more quantitatively, we define the ratio

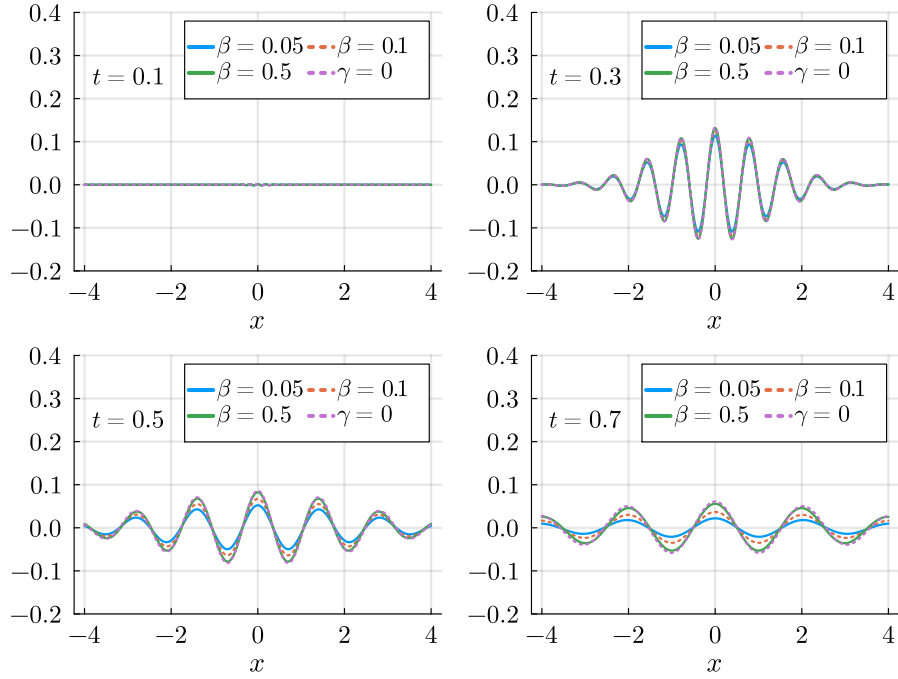
$$\mathcal{A}(t) = \frac{\rho_{01}(0, 0; t)}{\rho_{00}(0, 0; t)} = \exp \left\{ -\frac{1}{2}(k^2 + p^2)(K_4 - K_5) \right\} , \quad (5.26)$$

where  $k^2 + p^2 = 50^2 + 1 = 2501$  in our setup. In Fig. 12 (Top), we plot  $K_4 - K_5$  against  $t$  for various values of  $\gamma$  and  $\beta$ . In Fig. 12 (Bottom), we plot the rescaled quantity  $\frac{\beta}{\gamma}(K_4 - K_5)$  against  $t^2$ . We find that the data points lie on a straight line at early times, which implies that the ratio  $\mathcal{A}(t)$  decreases as  $\exp\{-c(\gamma/\beta)t^2\}$ . This  $O(t^2)$  behavior is different from the  $O(t)$  and  $O(t^3)$  behaviors observed in different parameter regimes [51].

Combining the direct terms and the interference term, we obtain the total reduced density matrix  $\rho_S(x, x; t)$  defined by (5.2). In Fig. 13 we plot it against  $x$  at  $t = 0.1, 0.3, 0.5$  and  $0.7$  for various  $\gamma$  with  $\beta = 0.05$  (a) and for various  $\beta$  with  $\gamma = 0.1$  (b). As we have seen in Fig. 9, the two wave packets in the direct terms start to overlap at  $t = 0.3$ . Correspondingly, we start to see a clear interference pattern at  $t = 0.3$ . At later times, the interference pattern tends to disappear for larger  $\gamma$  and higher temperature  $T = \beta^{-1}$  due to the effect of decoherence.



(a)  $\gamma$  dependence



(b)  $\beta$  dependence

**Figure 11:** The interference term  $\text{Re } \rho_{01}(x, x; t)$  is plotted for various  $\gamma$  with fixed  $\beta = 0.05$  (a) and for various  $\beta$  with fixed  $\gamma = 0.1$  (b). In the latter, the result for  $\gamma = 0$  is also shown for comparison.

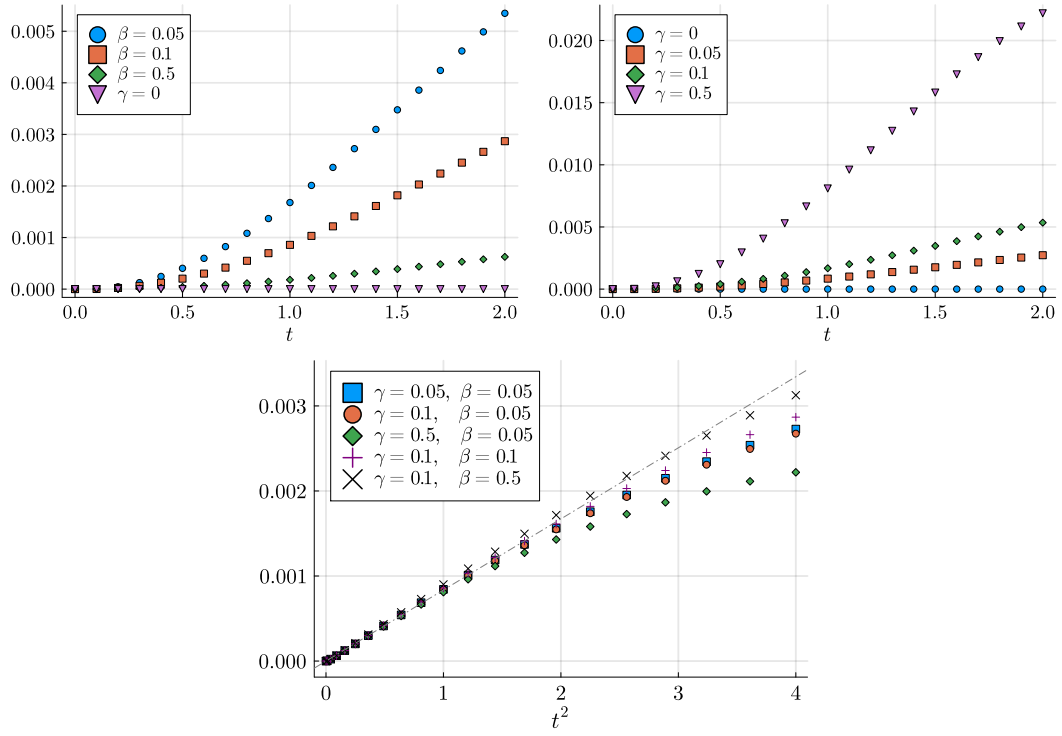
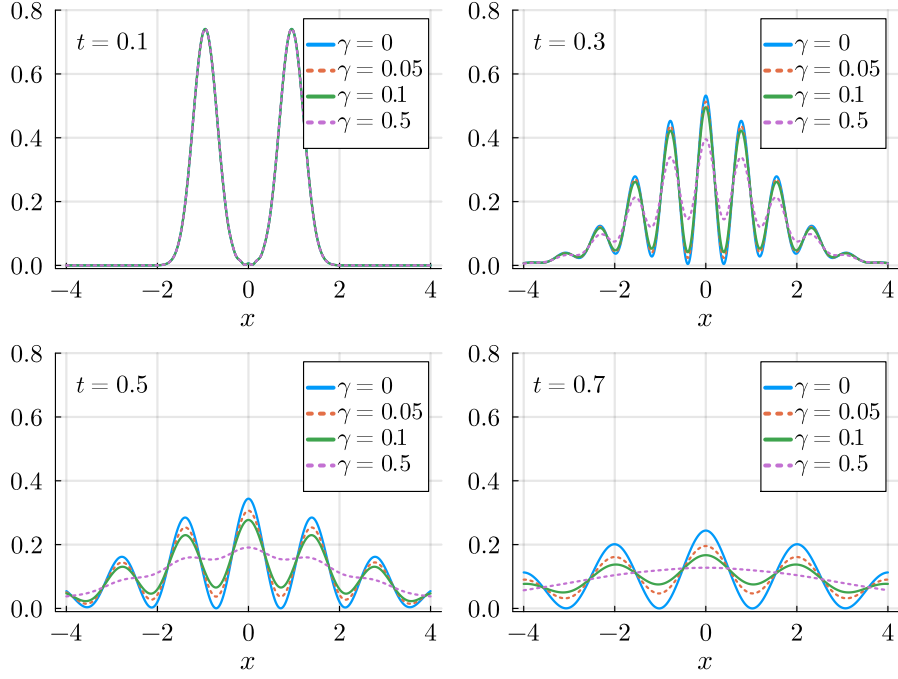
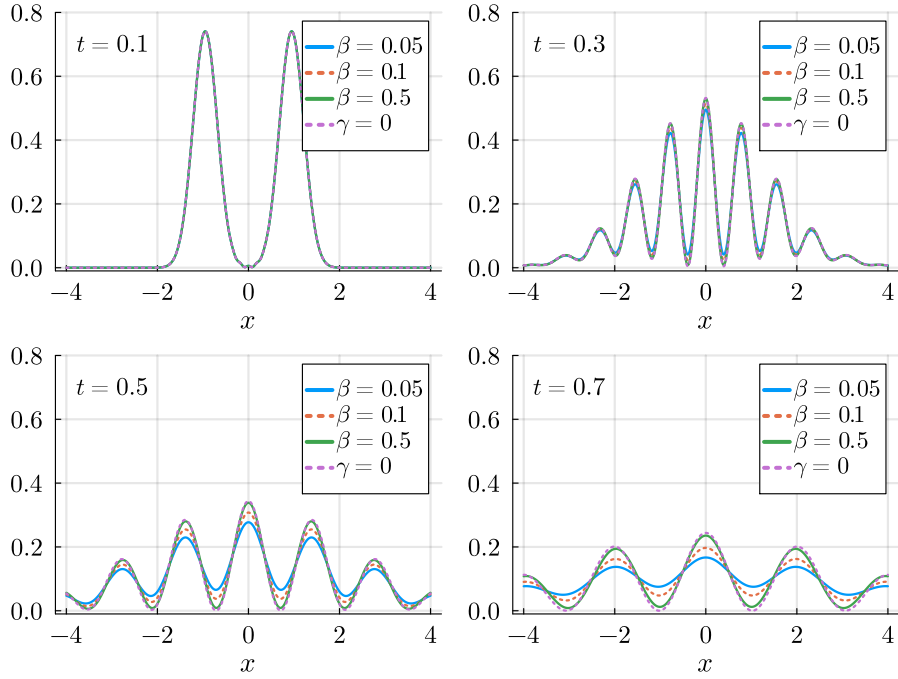


**Figure 12:** (Top) The quantity  $K_4 - K_5$  is plotted against  $t$  for various  $\gamma$  with  $\beta = 0.05$  (Left) and for various  $\beta$  with  $\gamma = 0.1$  (Right). (Bottom) The rescaled quantity  $\frac{\beta}{\gamma}(K_4 - K_5)$  is plotted against  $t^2$  for various  $\beta$  and  $\gamma$ .



(a)  $\gamma$  dependence



(b)  $\beta$  dependence

**Figure 13:** The total reduced density matrix  $\rho_S(x, x; t)$  is plotted against  $x$  for various  $\gamma$  with  $\beta = 0.05$  (a) and for various  $\beta$  with  $\gamma = 0.1$  (b). In the latter, the result for  $\gamma = 0$  is also shown for comparison.

## 6 Summary and discussions

In this paper we have investigated quantum decoherence numerically in the real-time path integral formalism. While this has been thought to be extremely difficult due to the sign problem that occurs in standard Monte Carlo methods, recent developments of numerical methods such as the GTM have made it possible practically. In particular, in the case of the Caldeira–Leggett model, which has been studied extensively as a model of quantum decoherence, we have pointed out that the GTM simplifies drastically since there is only a single relevant saddle point, which can be obtained numerically by solving a linear equation with a sparse coefficient matrix, and the integration over the Lefschetz thimble is nothing but the Gaussian integral around the saddle point, which can be done analytically. This enabled us to obtain the time-evolved reduced density matrix reliably even for a long time and for a large number of harmonic oscillators in the environment.

Unlike the previous works on the Caldeira–Leggett model, we were able to obtain explicit results for completely general parameters without any assumptions or approximations. In particular, we have succeeded in reproducing the scaling behaviors of the decoherence predicted from the master equation at weak coupling and at high temperature. We have also seen certain deviation from the predicted behavior by lowering the temperature. Furthermore, by increasing the degrees of freedom in the environment and by investigating the long-time evolution of the system, we were also able to see clear tendencies that the system of our interest thermalizes through the interaction with the environment, which plays the role of the heat bath.

Below we list some future directions. First of all, it is interesting to explore the parameter regimes that were not studied previously due to the limitation of the theoretical methods. For instance, our calculations do not rely on the Markov approximation, which implies that there is no obstacle in investigating the case in which the harmonic oscillators in the environment has a spectral density  $\rho(\omega) C^2(\omega) \propto \omega^p$  with  $p < 2$  (sub-Ohmic) or  $p > 2$  (super-Ohmic)<sup>13</sup>. Furthermore, in order to investigate a more realistic model of quantum decoherence, one can investigate a system with an anharmonic potential and/or with a non-Gaussian initial wave function by using the GTM [26–32]. We hope that the present work provides an ideal testing ground for such calculations.

Last but not the least, quantum decoherence discussed in this paper is expected to play a crucial role also in quantum-to-classical transition [1, 2]. For instance, it would be interesting to investigate the mechanism of the transition based on the environment-induced superselection [40, 53, 54] (See also [55, 56] and references therein for recent discussions.) by performing explicit calculations discussed in this paper.

### Acknowledgements

We would like to thank Yuhma Asano, Masafumi Fukuma, Kouichi Hagino, Yoshimasa Hidaka, Katsuta Sakai, Hidehiko Shimada, Kengo Shimada, Hideo Suganuma and Yuya Tanizaki for their helpful discussions and comments. H. W. was supported by Japan Society

---

<sup>13</sup>See Ref. [52] for previous work based on the master equation in this direction.

for the Promotion of Science (JSPS) KAKENHI Grant numbers, 21J13014, 22H01218 and 23K22489.

## A Discretization effects due to finite lattice spacing $\epsilon$ and finite $N_{\mathcal{E}}$

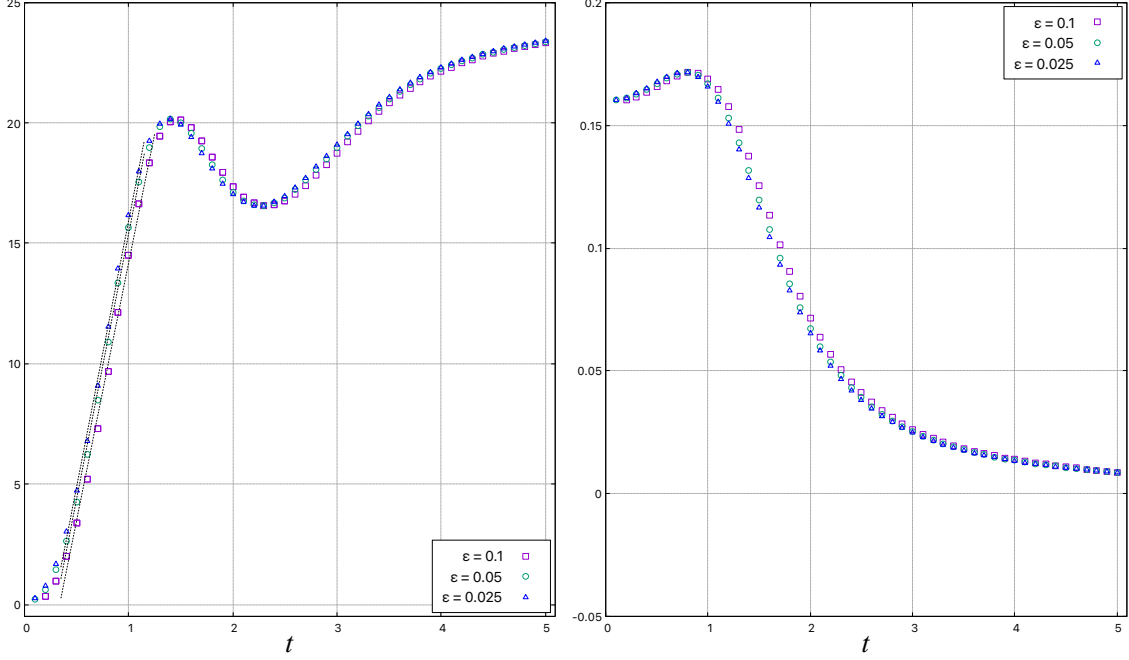


**Figure 14:** The quantities  $\Gamma_{\text{off-diag}}(t)$  (Left) and  $\Gamma_{\text{diag}}(t)$  (Right) are plotted against  $t$  for the lattice spacing  $\epsilon = 0.025, 0.05, 0.1$  with  $N_{\mathcal{E}} = 64$ ,  $\omega_{\text{cut}} = 2$ ,  $\beta = 0.05$  and  $\gamma = 0.1$  fixed. The dotted lines in the left panel represent fits to the behavior  $A \frac{16\gamma}{\beta} t + B$ .

In this appendix, we discuss the discretization effects due to finite lattice spacing  $\epsilon$  in time and finite  $N_{\mathcal{E}}$  in the environment.

In Fig. 14, we plot  $\Gamma_{\text{off-diag}}(t)$  (Left) and  $\Gamma_{\text{diag}}(t)$  (Right) against  $t$  for the lattice spacing  $\epsilon = 0.025, 0.05, 0.1$  with  $N_{\mathcal{E}} = 64$ ,  $\omega_{\text{cut}} = 2$ ,  $\beta = 0.05$  and  $\gamma = 0.1$  fixed. While we do see some  $\epsilon$  dependence, the value of the slope and the convergence to the thermal equilibrium are not drastically modified.

In Section 4.3, we have seen that the condition  $\omega_{\text{cut}} \gg \omega_r$  is important in the agreement with the prediction from the master equation. Here we note that  $N_{\mathcal{E}}$  has to be increased as we increase  $\omega_{\text{cut}}$  in order to regard the frequency spectrum (3.4) of the environment as continuous. In Fig. 15, we plot the quantity  $\Gamma_{\text{off-diag}}(t)$  against  $t$  for various choice of  $\omega_{\text{cut}}$  and  $N_{\mathcal{E}}$ . We find that the slope of the linear growth of  $\Gamma_{\text{off-diag}}(t)$  does not differ significantly between  $N_{\mathcal{E}} = 64$  and  $N_{\mathcal{E}} = 512$  for  $2 \leq \omega_{\text{cut}} \leq 8$ . Note, however, that the finite  $N_{\mathcal{E}}$  effect becomes more significant at late times as we can see in Fig. 3 (Left) due to the recurrence effects.

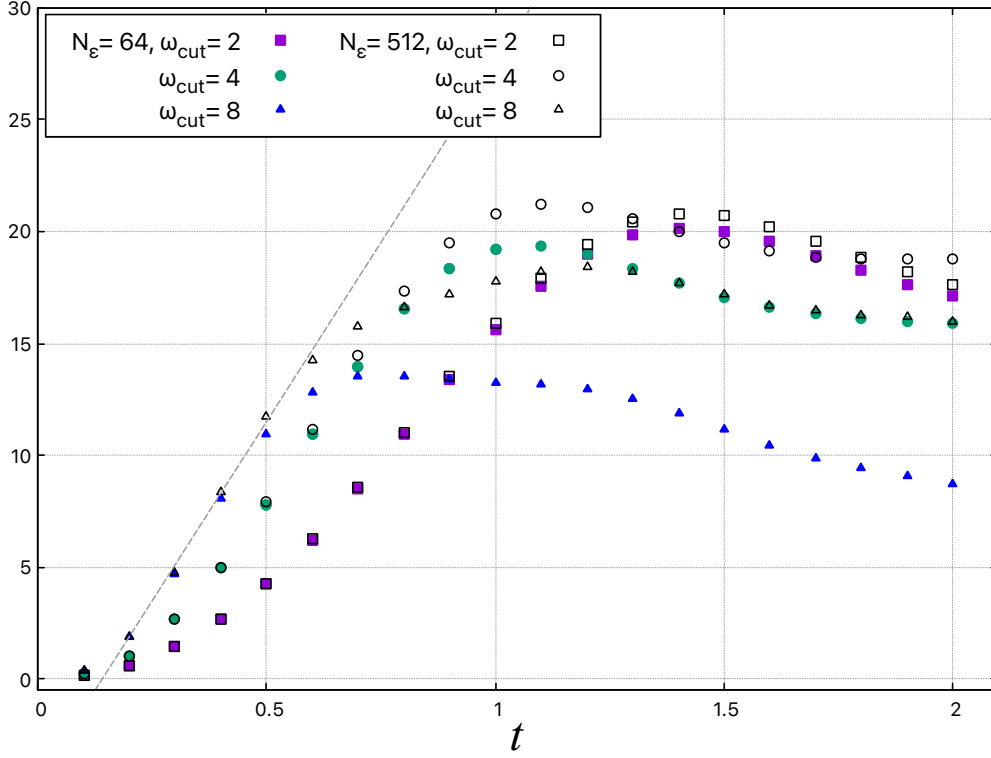


**Figure 15:** The quantity  $\Gamma_{\text{off-diag}}(t)$  is plotted against  $t \leq 2$  for various  $\omega_{\text{cut}} = 2, 4, 8$  and  $N_{\mathcal{E}} = 64, 512$  with  $\beta = 0.05$  and  $\gamma = 0.1$  fixed. The dashed line represents a guideline  $16\frac{\gamma}{\beta}t + \text{const}$  for the prediction from the master equation.

## B More on decoherence for two wave packets

In this appendix, we investigate the decoherence between the two wave packets discussed in Section 5 from a slightly different point of view. Here we pay attention to the off-diagonal elements of the reduced density matrix, which was discussed in the case of a single wave packet in Section 4.

For the off-diagonal elements of the reduced density matrix corresponding to  $x_F = -\tilde{x}_F = x$ , the exponent  $\mathcal{A}_{ab}$  that appears in (5.10) reduces to

$$\mathcal{A}_{ab} = \frac{1}{2}(c_\mu + \tilde{c}_\mu)(\mathcal{M}^{-1})_{\mu\nu}(c_\nu + \tilde{c}_\nu)x^2 - iE_\mu^{ab}(\mathcal{M}^{-1})_{\mu\nu}(c_\nu + \tilde{c}_\nu)x - \frac{1}{2}E_\mu^{ab}(\mathcal{M}^{-1})_{\mu\nu}E_\nu^{ab} . \quad (\text{B.1})$$

Thus each component of the density matrix is given by

$$\rho_{00}(x, -x; t) \simeq \exp \left\{ -\frac{1}{2}K_6 x^2 + i(kK_8 + pK_7)x + \frac{1}{2}(k^2K_4 - p^2K_5) \right\} , \quad (\text{B.2})$$

$$\rho_{11}(x, -x; t) = \rho_{00}(-x, x; t) , \quad (\text{B.3})$$

$$\rho_{01}(x, -x; t) \simeq \exp \left\{ -\frac{1}{2}K_6 x^2 - (kK_7 - pK_8)x + \frac{1}{2}(k^2K_5 - p^2K_4) \right\} , \quad (\text{B.4})$$

$$\rho_{10}(x, -x; t) = \rho_{01}(-x, x; t) , \quad (\text{B.5})$$

omitting the prefactors common to all components. We have defined the real quantities

$$K_6 = (c_\mu + \tilde{c}_\mu) \operatorname{Re}(\mathcal{M}^{-1})_{\mu\nu}(c_\nu + \tilde{c}_\nu) , \quad (\text{B.6})$$

$$K_7 = (e_\mu - \tilde{e}_\mu) \operatorname{Im}(\mathcal{M}^{-1})_{\mu\nu}(c_\nu + \tilde{c}_\nu) , \quad (\text{B.7})$$

$$K_8 = (e_\mu + \tilde{e}_\mu) \operatorname{Re}(\mathcal{M}^{-1})_{\mu\nu}(c_\nu + \tilde{c}_\nu) . \quad (\text{B.8})$$

We would like to see how the off-diagonal elements of the interference term  $\rho_{01}(x, -x; t)$  decrease with time. For that, we need to normalize the reduced density matrix by the normalization factor (5.24). The off-diagonal elements of the properly normalized reduced density matrix read

$$\begin{aligned} & \rho_{01}(x, -x; t) \\ &= \frac{1}{\mathcal{N}(t)} \exp \left\{ -\frac{1}{2} K_6 \left( x + \frac{kK_7 - pK_8}{K_6} \right)^2 + \frac{1}{2} \frac{(kK_7 - pK_8)^2}{K_6} + \frac{1}{2} (k^2 K_5 - p^2 K_4) \right\} . \end{aligned} \quad (\text{B.9})$$

In Fig. 16, we plot  $\rho_{01}(x, -x; t)$  against  $x$  for  $t = 0.1, 0.3, 0.5, 0.7$ . Note that we do not see the interference pattern unlike in Fig. 11 since we are looking at the off-diagonal components of the density matrix. We find that the amplitude is suppressed compared to the  $\gamma = 0$  case without the environment, and this suppression is stronger for larger  $\gamma/\beta$ .

In order to clarify the effect of decoherence more quantitatively, we calculate the peak height  $\rho_{01}(x, -x; t)$ , which is obtained as

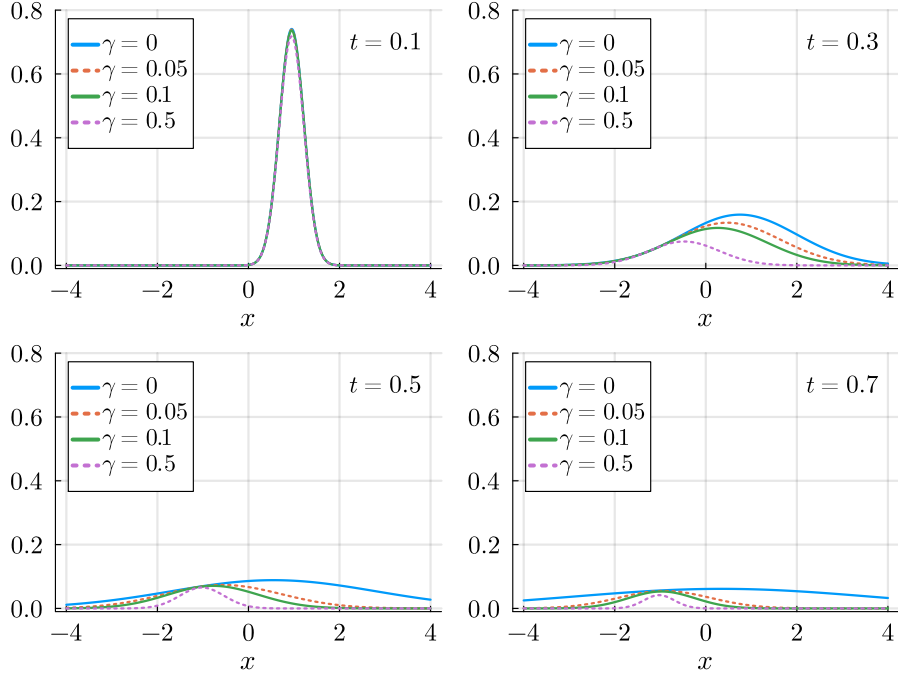
$$h(t) = \max_x \rho_{01}(x, -x; t) = \frac{1}{\mathcal{N}(t)} \exp \left\{ \frac{1}{2} \frac{(kK_7 - pK_8)^2}{K_6} + \frac{1}{2} (k^2 K_5 - p^2 K_4) \right\} . \quad (\text{B.10})$$

In Fig. 17, we plot  $-\log h(t)$  against  $t$  for various  $\gamma$  with  $\beta = 0.05$  (Left) and for various  $\beta$  with  $\gamma = 0.1$  (Right). Let us extract the effect of decoherence by considering the ratio  $R(t) \equiv h(t)/h(t)|_{\gamma=0}$ . In Fig. 18 we plot the quantity

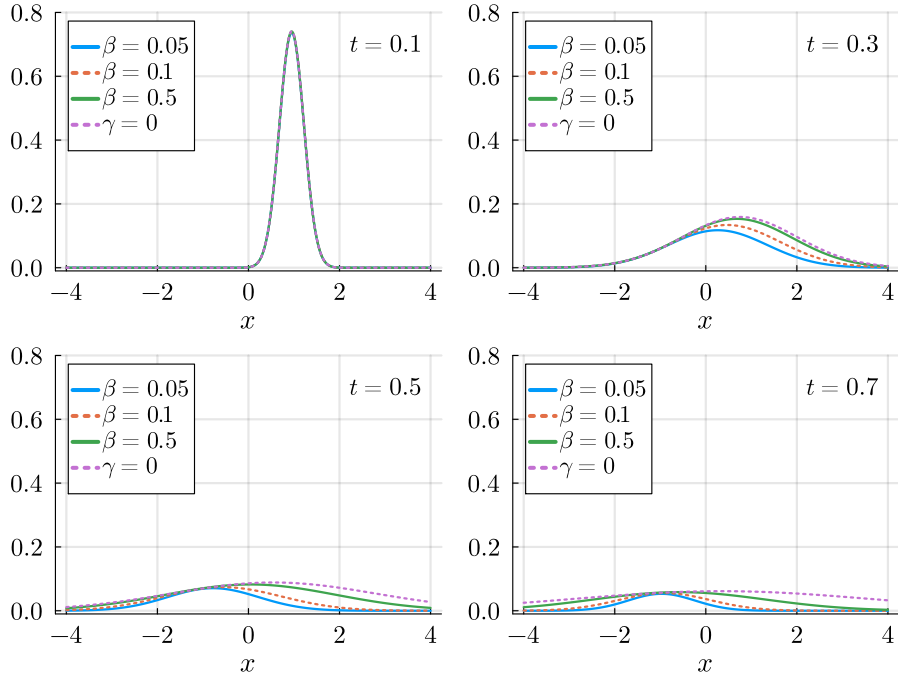
$$-\log R(t) = -\left( \log h(t) - \log h(t)|_{\gamma=0} \right) \quad (\text{B.11})$$

against  $t$ . The growth of this quantity at  $t \lesssim 0.2$  is faster for larger  $\gamma$  and for higher temperature  $T = 1/\beta$ . Fig. 19 shows that  $R(t) \sim \exp(-c(\gamma/\beta)t^2)$ , which is analogous to the behavior of (5.26). Thus we find that the effect of decoherence is visible also in the off-diagonal component of the density matrix although the effect is weaker than what we have seen in the interference pattern in Section 5.





(a)  $\gamma$  dependence



(b)  $\beta$  dependence

**Figure 16:** The off-diagonal elements of the interference term  $\rho_{01}(x, -x; t)$  is plotted at  $t = 0.1, 0.3, 0.5, 0.7$  for various  $\gamma$  with  $N_{\mathcal{E}} = 64$  and  $\beta = 0.05$  (Top) and for various  $\beta$  with  $N_{\mathcal{E}} = 64$  and  $\gamma = 0.1$  (Bottom). In the latter, the result for  $\gamma = 0$  is also shown for comparison.

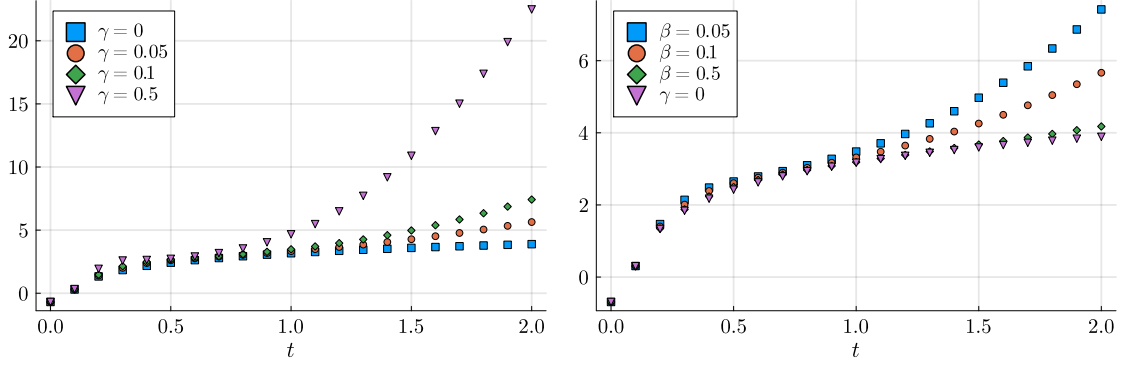
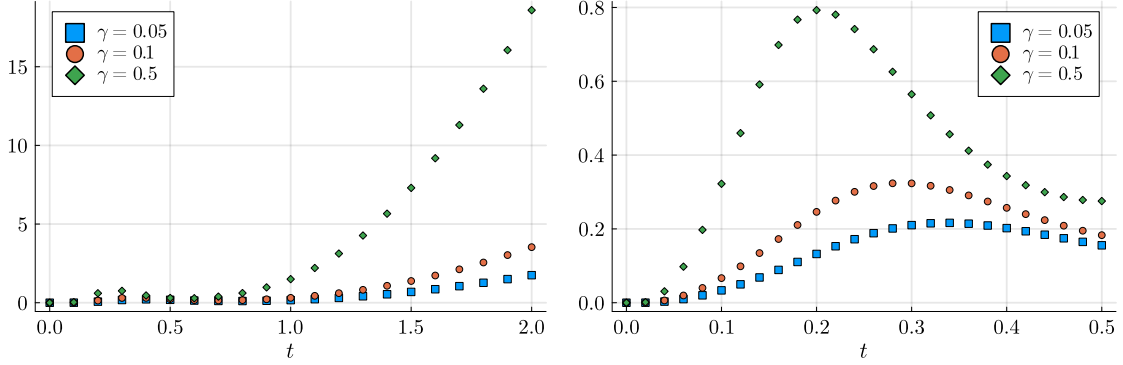
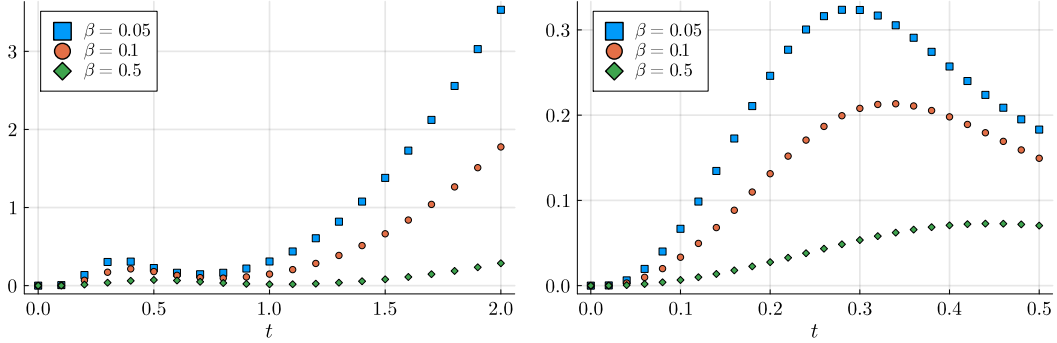


**Figure 17:** The quantity  $-\log h(t)$  with  $h(t)$  being the peak height of  $\rho_{01}(x, -x; t)$  is plotted against  $t$  for various  $\gamma$  with  $\beta = 0.05$  (Left) and for various  $\beta$  with  $\gamma = 0.1$  (Right). In the latter, the result for  $\gamma = 0$  is also shown for comparison.



(a)  $\gamma$  dependence



(b)  $\beta$  dependence

**Figure 18:** The quantity  $-(\log h(t) - \log h(t)|_{\gamma=0})$  is plotted for various  $\gamma$  with  $\beta = 0.05$  (Top) and for various  $\beta$  with  $\gamma = 0.1$  (Bottom). On the left, we show a longer time region  $0 \leq t \leq 2$  obtained with the lattice spacing  $\epsilon = 0.05$ , whereas on the right, we show a shorter time region  $0 \leq t \leq 0.5$  obtained with the lattice spacing  $\epsilon = 0.01$ .

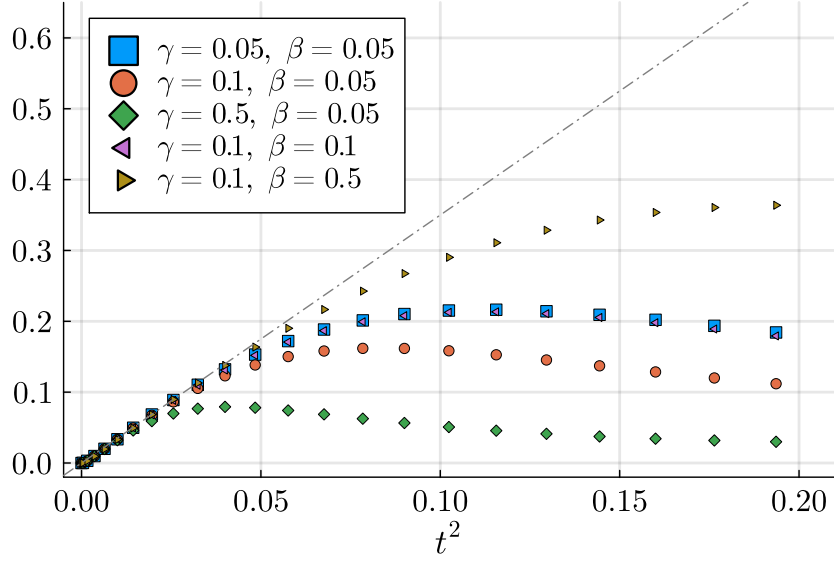


**Figure 19:** The rescaled quantity  $-\frac{\beta}{\gamma}(\log h(t) - \log h(t)|_{\gamma=0})$  is plotted against  $t^2$  for various  $\beta$  and  $\gamma$  with  $N_{\mathcal{E}} = 64$ . The dash-dotted line represents a fit to a linear behavior  $ct^2$  in the small- $t$  region.

## References

- [1] M. Schlosshauer, *Decoherence and the quantum-to-classical transition*. Springer Berlin, Heidelberg, 2007.
- [2] W. H. Zurek, *Decoherence and the transition from quantum to classical*, *Phys. Today* **44N10** (1991) 36 [[quant-ph/0306072](#)].
- [3] G. Lindblad, *On the generators of quantum dynamical semigroups*, *Commun. Math. Phys.* **48** (1976) 119.
- [4] V. Gorini, A. Kossakowski and E. C. G. Sudarshan, *Completely positive dynamical semigroups of  $N$  level systems*, *J. Math. Phys.* **17** (1976) 821.
- [5] C. Nagele, O. Janssen and M. Kleban, *Decoherence: A numerical study*, *J. Phys. A* **56** (2023) 085301 [[2010.04803](#)].
- [6] R. Adami and C. Negulescu, *A numerical study of quantum decoherence*, *Communications in Computational Physics* **12** (2012) 85–108.
- [7] C. Burrage, C. Kading, P. Millington and J. Minar, *Open quantum dynamics induced by light scalar fields*, *Phys. Rev. D* **100** (2019) 076003 [[1812.08760](#)].
- [8] C. Kading and M. Pitschmann, *New method for directly computing reduced density matrices*, *Phys. Rev. D* **107** (2023) 016005 [[2204.08829](#)].
- [9] C. Kading and M. Pitschmann, *Density matrices in quantum field theory: Non-Markovianity, path integrals and master equations*, [2503.08567](#).
- [10] S. Woodward, P. M. Saffin, Z.-G. Mou and A. Tranberg, *Optimisation of thimble simulations and quantum dynamics of multiple fields in real time*, *JHEP* **10** (2022) 082 [[2204.10101](#)].

- [11] J. Nishimura, K. Sakai and A. Yosprakob, *A new picture of quantum tunneling in the real-time path integral from Lefschetz thimble calculations*, *JHEP* **09** (2023) 110 [[2307.11199](#)].
- [12] K. Blum and O. Rosner, *Unraveling the bounce: a real time perspective on tunneling*, *2309.07585*.
- [13] D. Alvestad, A. Rothkopf and D. Sexty, *Lattice real-time simulations with learned optimal kernels*, *Phys. Rev. D* **109** (2024) L031502 [[2310.08053](#)].
- [14] T. Steingasser, M. König and D. I. Kaiser, *Finite-temperature instantons from first principles*, *Phys. Rev. D* **110** (2024) L111902 [[2310.19865](#)].
- [15] W.-Y. Ai, J. Alexandre and S. Sarkar, *False vacuum decay rates, more precisely*, *Phys. Rev. D* **109** (2024) 045010 [[2312.04482](#)].
- [16] T. Steingasser and D. I. Kaiser, *Toward quantum tunneling from excited states: Recovering imaginary-time instantons from a real-time analysis*, *Phys. Rev. D* **111** (2025) 096009 [[2402.00099](#)].
- [17] Z.-G. Mou, P. M. Saffin and A. Tranberg, *Computing real-time quantum path integrals on Sewed, almost-Lefschetz thimbles*, *JHEP* **03** (2025) 058 [[2410.12762](#)].
- [18] B. Garbrecht and N. Wagner, *False vacuum decay of excited states in finite-time instanton calculus*, *JHEP* **05** (2025) 076 [[2412.20431](#)].
- [19] J. Feldbrugge and J. Y. L. Jones, *Efficient evaluation of real-time path integrals*, *Phys. Rev. D* **111** (2025) 083524 [[2501.16323](#)].
- [20] A. H. Z. Kavaki and R. Lewis, *False vacuum decay in triamond lattice gauge theory*, *Phys. Rev. D* **112** (2025) 014502 [[2503.01119](#)].
- [21] E. Witten, *Analytic continuation of Chern-Simons theory*, *AMS/IP Stud. Adv. Math.* **50** (2011) 347 [[1001.2933](#)].
- [22] AURORASCIENCE collaboration, *New approach to the sign problem in quantum field theories: High density QCD on a Lefschetz thimble*, *Phys. Rev. D* **86** (2012) 074506 [[1205.3996](#)].
- [23] M. Cristoforetti, F. Di Renzo, A. Mukherjee and L. Scorzato, *Monte Carlo simulations on the Lefschetz thimble: Taming the sign problem*, *Phys. Rev. D* **88** (2013) 051501 [[1303.7204](#)].
- [24] H. Fujii, D. Honda, M. Kato, Y. Kikukawa, S. Komatsu and T. Sano, *Hybrid Monte Carlo on Lefschetz thimbles - A study of the residual sign problem*, *JHEP* **10** (2013) 147 [[1309.4371](#)].
- [25] A. Alexandru, G. Basar, P. F. Bedaque, G. W. Ridgway and N. C. Warrington, *Sign problem and Monte Carlo calculations beyond Lefschetz thimbles*, *JHEP* **05** (2016) 053 [[1512.08764](#)].
- [26] M. Fukuma and N. Umeda, *Parallel tempering algorithm for integration over Lefschetz thimbles*, *PTEP* **2017** (2017) 073B01 [[1703.00861](#)].
- [27] M. Fukuma, N. Matsumoto and N. Umeda, *Implementation of the HMC algorithm on the tempered Lefschetz thimble method*, *1912.13303*.
- [28] M. Fukuma and N. Matsumoto, *Worldvolume approach to the tempered Lefschetz thimble method*, *PTEP* **2021** (2021) 023B08 [[2012.08468](#)].
- [29] M. Fukuma, N. Matsumoto and Y. Namekawa, *Statistical analysis method for the worldvolume hybrid Monte Carlo algorithm*, *PTEP* **2021** (2021) 123B02 [[2107.06858](#)].

- [30] G. Fujisawa, J. Nishimura, K. Sakai and A. Yosprakob, *Backpropagating Hybrid Monte Carlo algorithm for fast Lefschetz thimble calculations*, *JHEP* **04** (2022) 179 [[2112.10519](#)].
- [31] M. Fukuma, *Simplified algorithm for the worldvolume HMC and the generalized thimble HMC*, *PTEP* **2024** (2024) 053B02 [[2311.10663](#)].
- [32] J. Nishimura, K. Sakai and A. Yosprakob, *Preconditioned flow as a solution to the hierarchical growth problem in the generalized Lefschetz thimble method*, *JHEP* **07** (2024) 174 [[2404.16589](#)].
- [33] C.-Y. Chou and J. Nishimura, *Monte Carlo studies of quantum cosmology by the generalized Lefschetz thimble method*, *JHEP* **05** (2025) 142 [[2407.17724](#)].
- [34] C.-Y. Chou, J. Nishimura and A. Tripathi, *Inequivalence between the Euclidean and Lorentzian Versions of the Type IIB Matrix Model from Lefschetz Thimble Calculations*, *Phys. Rev. Lett.* **134** (2025) 211601 [[2501.17798](#)].
- [35] A. O. Caldeira and A. J. Leggett, *Path integral approach to quantum Brownian motion*, *Physica A* **121** (1983) 587.
- [36] A. O. Caldeira and A. J. Leggett, *Quantum tunneling in a dissipative system*, *Annals Phys.* **149** (1983) 374.
- [37] W. G. Unruh and W. H. Zurek, *Reduction of a wave packet in quantum Brownian motion*, *Phys. Rev. D* **40** (1989) 1071.
- [38] J. P. Paz, S. Habib and W. H. Zurek, *Reduction of the wave packet through decoherence: How long does it really take?*, *Phys. Rev. D* **47** (1993) 488.
- [39] W. H. Zurek, S. Habib and J. P. Paz, *Coherent states via decoherence*, *Phys. Rev. Lett.* **70** (1993) 1187.
- [40] W. H. Zurek, *Decoherence, einselection, and the quantum origins of the classical*, *Rev. Mod. Phys.* **75** (2003) 715 [[quant-ph/0105127](#)].
- [41] M. Schlosshauer, *Quantum decoherence*, *Phys. Rept.* **831** (2019) 1 [[1911.06282](#)].
- [42] J. Nishimura and H. Watanabe, *Quantum Decoherence from Complex Saddle Points*, *Phys. Rev. Lett.* **134** (2025) 210401 [[2408.16627](#)].
- [43] L. Diósi and L. Ferialdi, *General non-markovian structure of gaussian master and stochastic schrödinger equations*, *Phys. Rev. Lett.* **113** (2014) 200403.
- [44] M. Schlosshauer, *Decoherence, the measurement problem, and interpretations of quantum mechanics*, *Rev. Mod. Phys.* **76** (2004) 1267 [[quant-ph/0312059](#)].
- [45] J. B. Hartle, *Space-time quantum mechanics and the quantum mechanics of space-time*, in *Les Houches Summer School on Gravitation and Quantizations, Session 57*, pp. 0285–480, 7, 1992, [gr-qc/9304006](#).
- [46] H. Grabert, P. Schramm and G. L. Ingold, *Quantum Brownian motion: The functional integral approach*, *Phys. Rept.* **168** (1988) 115.
- [47] R. P. Feynman and F. L. Vernon, Jr., *The theory of a general quantum system interacting with a linear dissipative system*, *Annals Phys.* **24** (1963) 118.
- [48] L. Diósi, *On high-temperature markovian equation for quantum brownian motion*, *Europhysics Letters* **22** (1993) 1.

- [49] L. Diósi, *Calderia-leggett master equation and medium temperatures*, *Physica A: Statistical Mechanics and its Applications* **199** (1993) 517.
- [50] A. O. Caldeira and A. J. Leggett, *Influence of dissipation on quantum tunneling in macroscopic systems*, *Phys. Rev. Lett.* **46** (1981) 211.
- [51] A. O. Caldeira and A. J. Leggett, *Influence of damping on quantum interference: An exactly soluble model*, *Phys. Rev. A* **31** (1985) 1059.
- [52] B. L. Hu, J. P. Paz and Y.-h. Zhang, *Quantum Brownian motion in a general environment: 1. Exact master equation with nonlocal dissipation and colored noise*, *Phys. Rev. D* **45** (1992) 2843.
- [53] W. H. Zurek, *Pointer basis of quantum apparatus: Into what mixture does the wave packet collapse?*, *Phys. Rev. D* **24** (1981) 1516.
- [54] W. H. Zurek, *Environment induced superselection rules*, *Phys. Rev. D* **26** (1982) 1862.
- [55] K. Konishi, *Quantum fluctuations, particles and entanglement: A discussion towards the solution of the quantum measurement problems*, *Int. J. Mod. Phys. A* **37** (2022) 2250113 [2111.14723].
- [56] K. Konishi, *Newton's equations from quantum mechanics for a macroscopic body in the vacuum*, *Int. J. Mod. Phys. A* **38** (2023) 2350080 [2209.07318].